## October 27, 2024

# ICE, CLOUD, AND LAND ELEVATION SATELLITE-2 (ICESat-2)

# Algorithm Theoretical Basis Document (ATBD) for ATL19/23 Gridded Dynamic Ocean Topography

Prepared By: ICESat-2 Science Definition Team Ocean Working Group

## **Contributors:**

James Morison David Hancock Suzanne Dickinson John Robbins Leeanne Roberts

## This document may be cited as:

Morison, J., D. Hancock, S. Dickinson, J. Robbins, and L. Roberts (2024). *Ice, Cloud, and Land Elevation Satellite (ICESat-2) Project Algorithm Theoretical Basis Document (ATBD) for Gridded Dynamic Ocean Topography Products, Version 4.* ICESat-2 Project, DOI: 10.5067//J3NTF6TM1SZ7



## **Abstract**

This document describes the theoretical basis of the ocean processing algorithms and the products that are produced by the ICESat-2 mission. It includes descriptions of the parameters that are provided in each product as well as ancillary geophysical parameters, which are used in the derivation of these ICESat-2 products.

## **CM** Foreword

This document is an Ice, Cloud, and Land Elevation Satellite-2 (ICESat-2) Project Science Office controlled document. Changes to this document require prior approval of the Science Development Team ATBD Lead or designee. Proposed changes shall be submitted in the ICESat-II Management Information System (MIS) via a Signature Controlled Request (SCoRe), along with supportive material justifying the proposed change.

In this document, a requirement is identified by "shall," a good practice by "should," permission by "may" or "can," expectation by "will," and descriptive material by "is."

Questions or comments concerning this document should be addressed to:

ICESat-2 Project Science Office Mail Stop 615 Goddard Space Flight Center Greenbelt, Maryland 20771

## **Preface**

This document is the Algorithm Theoretical Basis Document for the processing open ocean data to be implemented at the ICESat-2 Science Investigator-led Processing System (SIPS). The SIPS supports the ATLAS (Advance Topographic Laser Altimeter System) instrument on the ICESat-2 Spacecraft and encompasses the ATLAS Science Algorithm Software (ASAS) and the Scheduling and Data Management System (SDMS). The science algorithm software will produce Level 0 through Level 4 standard data products as well as the associated product quality assessments and metadata information.

The ICESat-2 Science Development Team, in support of the ICESat-2 Project Science Office (PSO), assumes responsibility for this document and updates it, as required, as algorithms are refined or to meet the needs of the ICESat-2 SIPS. Reviews of this document are performed when appropriate and as needed updates to this document are made. Changes to this document will be made by complete revision.

Changes to this document require prior approval of the Change Authority listed on the signature page. Proposed changes shall be submitted to the ICESat-2 PSO, along with supportive material justifying the proposed change.

Questions or comments concerning this document should be addressed to: Tom Neumann, ICESat-2 Project Scientist Mail Stop 615 Goddard Space Flight Center Greenbelt, Maryland 20771

## Review/Approval Page

## Prepared by:

Jamie Morison Senior Principal Oceanographer Affiliate Professor, Oceanography University of Washington, Applied Physics Laboratory

## Reviewed by:

Steve Nerem Professor Associate Director of Colorado Center for Astrodynamics Research University of Colorado, Boulder

Laurie Padman Senior Scientist President Earth & Space Research

## Approved by:

Tom Neumann Project Scientist, ICESat-2 NASA Goddard Spaceflight Center, Code 615

<sup>\*\*\*</sup> Signatures are available on-line at: https:///icesatiimis.gsfc.nasa.gov \*\*\*

# **Change History Log**

Revision Level	Description of Change	SCoRe No.	Date Approved
	Initial Release (11/9/2020 – Section 5.6.3.2.1 regarding equation 48 description, changed "cross product" to "product sum") The last ATL12 ATBD with a complete ATL19 description is ICESat2_JMdraft_Ocean_atbd_12012020_SD dated Jan. 4, 2021. Changes to ATL19 prior to 11/09/2020 are included in that ATL12 ATBD dated 12/30/2020, ICESat2_JMdraft_Ocean_atbd_12302020_CX. Changes to ATL19 ATBD from 12/3/2020 through 12/30/2020 were not tracked or logged and this ATBD originating as Morison's: ATL12 ATBD ICESat2_JMdraft_Ocean_atbd_12302020_CX should be considered the original ATL19 ATBD,  02/04/2021 Globally corrected grid_lon and grid_lat to lon_avg and lat_avg  02/04/2021 Corrected the anomaly equations at the end of the first paragraph of Appendix B by multiplying by (1/N)  02/22/2021 Finish global change of dof_grid to dof  02/22/2021 Section 3.2.4.2 correct dot_sigma_dfw_albm to		
	dot_sigma_dfwalbm  02/22/2021 global change of dot_dfwallbeam to dot_dfwalbm  02/22/2021 global change of dot_dfw_uncertain to dot_dfw_uncrtn  02/22/2021 Section 3.2.3.1.1 added computation of uncertainty in simple averages of DOT:  "To compute the uncertainty, dot_avg_uncrtn, in gridded DOT, dot_avg, divide dot_sigma_avg by the square root of dof to establish the uncertainty in the degree-of-freedom weighted DOT."  Also added dot_avg_uncrtn to Table 2  02/25/2021 In Table 2 corrected description of dot_avgcntr to "Simple average of dynamic ocean topography interpolated center of grid cell"  03/01/2021 In equation 49 corrected the equation for C to		

 $c = dot_avg - (a*lon_avg + b*lat_avg)$ 

04/14/2021 to 4/26/2021 – Numerous small corrections to make variable names consistent throughout

04/21/2021 – Section 3.2 Reordered and expanded to:

- 3.2 Gridding DOT and SSH for ATL19
- 3.2.1 The Grids
- 3.2.2 Temporal Averaging
- 3.2.3 Input to Gridding
- 3.2.4 Gridding
- 3.2.5 Gridding Output

and

Expand Introduction to include possible ice parameters and optimal interpolation considerations:

- 1.0 INTRODUCTION and Background
- 1.1 Background: ATL03 and ATL12
- 1.2 ATL19 Gridded Product
- 1.2.1 ATL19 Grids
- 1.2.2 The Basic Product
- 1.2.3 The running 3-month average
- 1.2.4 Merging with ATL10 to produce global DOT
- 1.2.5 Optimal interpolation of DOT

04/23/2021 Table 2 – Added "\_albm" variables

04/25/2021 Added Appendix E: Optimal Interpolation of ICESat-2 Dynamic Ocean Topography

4/29/2021 Numerous edits for clarity in response to David Hancock's comments

04/30/2021 – Added Figures 2-6 and related discussions

- Changed Table 2 to Table 3
- Added a new Table 2 listing inter-beam biases

6/23/2021 Section 3.2.3.1 Pre-grid filtering was changed to a single pass over ATL12 ocean segments rejecting any ocean segment with average DOT departing from the 10-degree latitude, all-ATL12 average DOT by more than three times the all-ATL12 standard deviation of DOT.

9/3/2021 Completed numerous edits suggested by reviewers Laurie Padman and Steve Nerem. This included adding ATL12 background and ATL19 rationale in revised introduction. The noteworthy conceptual addition not mentioned by reviewers was clarifying that the higher moments and uncertainty that are gridded represent only the sea state induced variances and that determining ocean segment-to-segment variability should be addressed with TBD methods.

9/4/2021 Added *meanoffit2* and *ds\_y\_bincenters* to Table 1 Inputs from ATL12 and added *dot\_hist*, *dot\_hist\_albm*, and *ds\_y\_bincenters* to Table 3 Outputs

9/4/2021 Changed *dot\_hist\_grid* to *dot\_hist* throughout and changed description of calculation of *dot\_hist* to:

"To compute the bin aggregate probability density function (PDF), dot\_hist, of DOT, we first must convert each Y PDF from ATL12 to a PDF of DOT by adding meanoffit2 to the x-axis of Y, ds\_y\_bincenters and then interpolating the result to an intermediate PDF, Yintermediate, evaluated at the original ds\_y\_bincenters. (Note: In ATL19 Release 1, meanoffit2 was inadvertently not added so the aggregate histograms only reflect the aggregate wave environment with mean near zero). The aggregate probability PDF, dot\_hist, of DOT will equal the sum Yintermediate x n\_photons in each histogram bin of all Yintermediate divided by the total, n photons gridttl, of all n photons."

2/8/2022 In Section 3.2.3 changed the DOT to be averaged for all products to include the sea state bias correction equal to subtracting the ATL12 ocean segment average of SSB, i.e., dot=h-geoid\_seg-bin\_ssbias

2/8/2022 Modified Section 3.2.4.4.1 and Table 3 to:

- 1) Remove "cntr" averages of depth, geoid and SWH and change *ssb\_avgcntr* to a value interpolated to the center using the *a*, *b*, *c* coefficients for *dot\_avgcntr*, now called *a\_avg*, *b\_avg*, and *c\_avg*
- 2) Called for saving and outputtin a avg, b avg, and c avg
- 3) Modified the editing criteria to comparing *QoF* to the departure of the 9-cell average of DOT from DOT interpolated to the average of ocean segment positions in the 9 cells

## 2/8/2022 Modified Section 3.2.4.4.2 and Table 3 to:

- 1) Remove "cntr" dfw averages of depth, geoid and SWH and change *ssb\_dfwcntr* to a value interpolated to the center using the *a, b, c* coefficients for *dot\_dfwcntr*, now called *a\_dfw*, *b\_dfw*, and *c\_dfw*
- 2) Called for saving and outputtin *a\_dfw*, *b\_dfw*, and *c\_dfw* Modified the editing criteria to comparing *QoF* to the departure of the 9-cell dfw average of DOT from DOT interpolated to the dfw average of ocean segment positions in the 9 cells

2/11/2022 Edited 3.2.4.4.1 and 3.2.4.4.2 To eliminate variable names that would duplicate exiting variable names and worked to clarify the procedure to calculate dfw and average center values.

02/11/2022 In 3.2.4.4.1 and 3.2.4.4.2 changed the derivation of *ssb\_avgcntr* and *ssb\_dfwcntr* to the difference between DOT calculated with and without the SSB correction.

02/14/2022 In 3.2.4.4 first paragraph, changed:

a minimum of three ocean segments in the cell to compute a center-interpolated DOT value." to

"a minimum of four ocean segments in the cell to compute a center-interpolated DOT value."

2/17/2022 In 3.2.4.4.1.1 and 3.2.4.4.2.2 corrected all *a* coefficients to multiply times longitude and *b* coefficients times latitude. Also *DOT-avgnobias* corrected to *DOT\_avgnobias* and *DOT-dfwnobias* corrected to *DOT\_dfwnobias*.

2/24/2022 In 3.2.4.4.1.1 and 3.2.4.4.2.2 changed the editing criteria for center values to

Edit the centered average values according to the following criteria related to the variation of DOT across the cell and the quality of the linear fit. For center cells with an average DOT, dot\_avg\_albm, remove values of dot\_avgcntr when

 $abs (\textit{dot\_avg\_albm -(a\_avg*lon\_avg + b\_avg*} \\ lat\_avg+c\_avg)) > 2*QoF$  (51)

where  $QoF = RMS (DOT\_seg - a\_avg*lon\_seg + b\_avg*lat seg+c avg),$ 

and

Edit the centered average values according to the following criteria related to the variation of DOT across the cell and the quality of the linear fit. For center cells with an average DOT, **dot dfw albm**, remove values of **dot dfwcntr** when

abs 
$$(dot\_dfw - (a\_dfw*lon\_dfw + b\_dfw* lat\_dfw + c\_dfw))$$
  
>  $2*QoF$  (55)

where  $QoF = RMS (DOT\_seg - a\_dfw*lon\_seg + b\_dfw*lat\_seg + c\_dfw)$ ,

2/24/2022 In 3.2.4.4.1.1 and 3.2.4.4.2.2 edited to specify that centered values would be computed using all beams in the 9-cell cluster.

2/24/2022 In Table 3 specified centered average and dfw averaged sea state bias would be calculated as specified in the ATBD.

2/24/2022 In Table 3 eliminated dot\_avgcntr\_albm, dot\_dfwcntr\_albm, ssb\_avgcntr\_albm, and ssb\_avgcntr\_albm as redundant with dot\_avgcnt, dot\_dfwcntr, ssb\_avgcntr, and ssb\_avgcntr computed with all-beam data.

3/8/2022 Added ice concentration, ice\_conc, to variables such as depth to be averaged in single beam and all beam data. Added to Table 1 Inputs, Section 3.2.4.2.1, and Table 3 Outputs

3/8/2022 Where the criteria for editing "\_cntr" interpolated values for grid cells without a dot\_avg had been TBD, changed the criteria to "QoF is greater than 0.2 m, a value estimated from examination of distributions of OoF to exceed more than 95% of OoF values"

4/5/2022 Corrected Table 3 for consistent treatment of variable

names and consistency with ATL19 data files: Added "\_" albm to dot dfw uncrtn in Table3

Added "\_"\_albm to dot\_hist and deleted row for dot\_hist\_albm in Table 3 consistent with formatting of other albm variable mentions in the table.

Corrected name surf\_prcnt\_avg \_albm in Table 3 consistent with formatting of other *albm* variable mentions in the table

Added row for *surf\_prcnt\_dfw* and *surf\_prcnt\_dfw"\_"*\_albm to Table 3

Added *popped\_flag* variables to Table 1 and Table 3 and a short paragraph at the beginning of Section 3.2.3.1:

"The ATL12 ocean segment data going into ATL19 are already filtered for depths greater than 10-m and for pointing and orbit determinations outside of nominal conditions (ATL03 podppd flag = 0, nominal, or 4, nominal calibration maneuver). Ocean segment averages of depth, depth\_seg, and the highest of the podppd flag used in an ocean segment, podppd\_flag\_seg, are included in ATL12 output. ATL19 gridded averages of these quantities are computed as discussed below and in Table 3."

Deleted the sea ice flag row and TBD from Table 3 because we now have ice concentration.

4/20/2022 In table 3, modified the description of *surf\_type\_prcnt* to better explain it as: "The percentages of each *surf\_type* of the photons in the ocean segment as a 5-element variable with each element corresponding to the percentage of photons coming from positions under each of the 5 surface masks. Due to mask overlaps, photons can originate from more than one mask type, and the 5 surface type percentages can total more than 100%.

5/15/2022 - In Section 3.2.4.4.1 added calculation of uncertainty in DOT average at the cell center position, *dot\_avgcntr\_uncrtn*, based on temporary appendix F and specified *dot\_avgcntr\_uncrtn* as the editing criteria for center values in place of *QoF*. Also add *dot avgcntr\_uncrtn* to Table 3, and added Appendix F. Appendix F

can be substituted for Appendix C once *dot\_avgcntr\_uncrtn* is successfully implemented and checked.

5/17/2022 – In section 3.2.4.4.1 corrected parentheses mistake in equation for **QoF** and simplified editing to discard any **dot\_avgcntr** values for which the **dot\_avgcntr\_uncrtn** exceeds TBD m = 0.2m in initial tests

5/31/2022 – In Section 3.2.4.4.1, equation 14F, corrected parentheses mistake and substituted Lxx for Lyy in the uncertainty of b term. Other small edits for clarity.

6/16/2022 – Incorporated the uncertainty calculation portion of what had been **Appendix F** into **Appendix B** and changed the normalization of (B8), which had been (F8) from 1/(N-3) to 1/(N-2). In the body of the ATBD the calculation of **QoF** was changed to reflect the uncertainty as calculated according to (B8), and numerous formatting and minor editorial changes were also made.

6/16/2022 – Also in 3.2.4.4, added a paragraph justifying the inclusion of a land mask, *landmask*, equal to 1 to indicate if a cell center point was on land. Also added *landmask* to the output table, Table 3.

6/17/2022 – Discussion surrounding equation (55) grayed out pending development of uncertainty for dfw variables. Hierarchy, Page 42, (under ATL12 inputs to ATL19), changed SSH-geoid\_seg to SSH-geoid\_seg-bin\_ssbias.

Page 42 (3.2.4.4.1 and 3.2.4.4.2) Removed the centered values we no longer calculate, keeping only dot and ssb.

Page 42 (3.2.3.2.2), changed grid\_lat\_dfw to lat\_dfw

Page 42 (3.2.3.2.2), changed grid\_lon\_dfw to lon\_dfw

Page 43 (3.2.4.2.1), changed surf\_avg to surf\_prcnt\_avg

6/25/2022 – Changed variable name *land\_mask* to *landmask* throughout

6/25/2022 – In Appendix B, added with editing for style section **B.2 Degree-of-Freedom-Uncertainty Weighted Average DOT** from John Robbins write up of weighted least square. 6/21/2022.

6/25/2022 – Changed 3.2.4.2.2 to Averaging Weighted by Degrees-of-Freedom-Uncertainty and changed all the dfw averages from

averages weighted by DOF =  $np\_effect$  to averages weighted by  $Wi = (1/h\_uncrtn)^2$ . Also added explanation that because this weight is equal to  $np\_effect/dot\_sigma$  it includes the effect of wave amplitude as well as degrees-of-freedom on uncertainty, and the resulting averages weighted by Wi should have the minimum uncertainty. The dfw variable names were not changed but are referred to generically in the text as degree-of-freedom-uncertainty weighted variables (same acronym, slightly different meaning)

6/25/2022 – Made separate Section 3.2.4.4.2 for centered dfw averages weighted Wi and including uncertainty for the dot\_dfwcntr values according to the Robbins write up in Appendix B.2.

6/28/2022 - Numerous edits suggested by John Robbins and David Hancock to identify ATL23 as the 3-month moving average gridded product.

7/12/2022 – Ice concentration averages output, *ice\_conc\_avg*, name has been contracted to *ice\_conc* in <u>3.2.4.2.1</u> consistent with Table 3.

7/12/2022 – Changed headers and footers to Rel. 003. Summer 2022.

7/12/2022 – This is meant to be the same ATBD as ICESat2\_ATL19\_atbd\_06282022 with a few of the added edits by Suzanne Dickinson added to the 6/25/2022 version to make what we are calling ICESat2\_ATL19\_atbd\_06182022 to issue with ATL19/23 Rel. 003, V. 01. Specifically, this version has the dfw degree-of-freedom weighted averaging weighted by *np\_effect* converted to degree-of-freedom-uncertainty weighted averaging weighted by Wi equal to (1/h\_uncrtn)². This version will be the future basis of the ATBD development.

7/29/2022 – In section 3.2.4.2.1 modified description of the aggregate histogram calculation and definition of **dot\_hist** to include **ds\_hist\_bincenters** thusly: **. dot\_hist** extends over bins centered **ds\_hist\_bincenters** that are the same as **ds\_y\_bincenters** truncated to  $\pm$  3m. (Note: In ATL19 Release 2, **ds\_hist\_bincenters** is referred to as **ds\_grid\_dot**.)

8/4/20022 – Correction to the above changed: "truncated to  $\pm$  3m. (Note: In ATL19 Release 2, *ds\_hist\_bincenters* is referred to as *ds\_grid\_dot*.)" to: ", i.e.,  $\pm$ 15m"

7/29/2022 – In Table 1 moved *ds\_y\_bnicenters* to the top of the table and eliminated and deleted *ancillary data* group.

7/29/2022 – Added to Table 3 ds\_hist\_bincenters with mention of (ds grid dot in Release 2).

8/4/2022 – Deleted mention of "(ds grid dot in Release 2)."

7/29/2022 – Added to the Table 3 description of *dot\_hist* and *dot\_hist\_albm*, "Histogram bin centers are given by *ds\_hist\_bincenters*. (*ds\_grid\_dot in Release 2*)" 8/4/2022 –In Table 3: Deleted mention of "(*ds\_grid\_dot in Release 2*)."

8/4/2022 – In Table 3: Moved variable dimension for bins in dot\_hist\_albm to first position.

8/4/2022 – In Table 3: To reduce data storage, eliminate *dot\_hist*, keeping only *dot hist albm* 

8/4/2022 – At the end of Section 3.2.4.2.1: Added the paragraph to say only computing dot\_hist\_albm,

"Note that in the implementation of Release 2 of ATL19, we found that including *dot\_hist* for each individual, beam each grid cell, and 6001 histogram bins used an excessive amount of storage necessitating the computation of *dot\_hist* only as an aggregate for all beams termed *dot\_hist albm.*"

8/4/2022 – In Table 3: Removed dot\_hist leaving only dot\_hist\_albm with description: "All beam aggregate probability density function of DOT histograms (ATL12 *Y* histogram + *measnoffit2*). Histogram bin centers are given by *ds\_hist\_bincenters* for each of the three grids."

9/20/2022 – In Section 3.2.4.4.2 eliminated extraneous  $W_i$  multiplier from equation 52, 52b, 53, and 54 to be consistent with Appendix B. Also referred to Section 3.2.4.2.2 for calculation of averages *lat\_dfw9*, *lon\_dfw9*, and *dot\_dfw9* used in equation 52, 52b, 53, and 54.

8/17/2023 Specify outputting *dot\_dfwcntr\_uncrtn* in *Section* 3.2.4.4.2 and *Table 3* 

9/28/2023 Made extensive modifications to 1.2./4, 3.2.3.1 and

3.2.4.2.2 to incorporate *h\_ice\_free* to yield DOT in ice-covered waters, ATL07 provide a flag in ATL12 10-m bins indicating the presence of bright leads and *h\_ice\_free* is the average of the *htybin* in these bright lead 10-m bins. Generally, we propose that *h\_ice\_free* be substituted for *h-geoid\_seg* whenever it appears and *h-geoid\_seg* be taken to represent the top of the ice, *h\_icetop\_geoid*, when ice concentration is greater than 15%, A small number of variables have been added to outputs, but the previous processing routines can be left unchanged if we can make the substitution of *h\_ice\_free* where it exists for *h-geoid\_seg*.

11/16/2023 Added notes to the **dfw** and **dfw9** average descriptions to the effect of substituting **h\_ice\_free\_uncrtn** for **h\_uncrtn** wherever we are substituting **h\_ice\_free** for **h-geoid\_seg** in ice-covered conditions, i.e., (Note: In ice covered waters, **ice\_conc**> or equal to 15%, where we substitute **h\_ice\_free** for **h-geoid\_seg**, we will also substitute the uncertainty in **h\_ice\_free**, **h\_ice\_free\_uncrtn**, for the uncertainty in **h, h\_uncrtn**. This will be critically important in the averaging schemes weighted by uncertainty for **dot\_dfw9** and companion **dfw9**-averaged variables).

11/16/2023: In Table 1 of Inputs, deleted *ice conc 07icefree* because it couldn't be calculated in a meaningful way given the overlap of ATL07 sea ice segments.

11/16/2023: In output Table 3 and in text replaced *h ATL07 ice free* with *h atl07 ice free*.

11/16/2023: In output Table 3 and in text replaced *hicefree\_std\_ice\_free* with *h\_ice\_free\_uncrtn*.

11/16/2023: In Table 3 of outputs deleted dot\_avginice\_07 and dot\_avginice\_7in12 as redundant with h\_atl07\_ice\_free and h\_atl07\_inatl12ocavg\_albm

11/20/2023: Corrected the above to specify that in Sections 1.2.4

11/20/2023: Corrected the above to specify that in Sections 1.2.4 and 3.2;.3.1: *dot\_avginice\_07* and *dot\_avginice\_07\_albm* and *dot\_avginice\_7in12* and *dot\_avginice\_7in12* be the averages and all-beam averages of *h\_atl07\_ice\_free* and *h\_atl07\_inatl12oc* 

Also modified description of *dot\_avginice\_07* and *dot\_avginice\_07\_albm* to be: "Simple average of dynamic ocean topography in sea ice based ATL07 DOT in bright lead ATL07 segments that make ATL12 10-m bins fully covered."

11/21/2023: Deleted *h\_atl07\_ice\_free\_avg\_albm* and *h\_atl07\_inatl12ocavg\_albm* from Table 3

11/25/2023: In Figure 2, corrected caption.

11/25/2023: In 3.2.4.2.2, specified:

"For all the ATL12 ocean segments in each month to be gridded that have sea ice data, we will compute  $h\_bias12rel07$  equal to the difference between  $h\_ice\_free$  and  $h\_atl07\_ice\_free$  in 5% ice concentration bins, e.g., 15% to  $\leq 20\%$ ,  $\geq 20\%$  to  $\leq 25\%$ , ...  $\geq 95\%$  to  $\leq 100\%$  with bin centers as bin lables."

11/25/2023: Added to Table 3 descriptions of dfw variables distinction per description for  $dot\_dfw$ , of weighting by  $h\_unctn$  for IC<15%, and  $h\_ice\_free\_uncrtn$  for IC>15% and use of  $h\_ice\_free$  in lieu of  $h\_geoid\_seg\_ssbias$  for ice concentration  $\geq$ 15%

11/28/2023: Applied Leeanne Robert's corrections and edits to Table 3.

12/21/2023 In sections 1.2.4, 3.2.3.1, 3.2.4.2.2, and 3.2.4.2.4 Added specifications for 3 ice concentration categories: IC<15 % for DOT use *h-geoid\_seg-bin\_ssbias*15% ≤IC≤70 % for DOT use *h\_ice\_free*IC>70 % for DOT use *h\_atl07\_inatl12oc*and the related uncertainties.

And for IC $\geq$ 15% add simple averages for *h\_ice\_free*, *h\_atl07\_ice\_free*, and *h\_atl07\_inatl12oc*, with respective uncertainties and related sea ice pertinent variables.

12/21/2023 - Everywhere corrected *h-geoid\_seg* or *h-geoid\_seg-ssb\_seg*, with *h-geoid\_seg-bin\_ssbias* 

2/27/2024 - Modified **1.2.4 2**) and **3.2.3.1 2**) to, "Or if *h\_ice\_free* does not exist (is invalid) but *h\_atl07\_inatl12oc* does exist, *h\_atl07\_inatl12oc* will be substituted for the open ocean DOT variable, *h-geoid\_seg-bin\_ssbias*, in the gridding process, and if *h\_atl07\_inatl12oc\_uncrtn* exists it will be substituted for *h\_uncrtn* as the DOT uncertainty in the gridding processes, or if

 $h_atl07_inatl12oc\_uncrtn$  does not exist, a fixed empirical uncertainty, e.g.,  $\pm$  5 cm, will be substituted for  $h_acrtn$  as the DOT uncertainty in the gridding processes."

2/27/2024 - Modified **3.2.3.1** just below figure 6 to specify the uncertainty in h\_icetop\_geoid, "The uncertainty in h\_icetop\_geoid, h icetop geoid uncrtn, will be h uncrtn for  $IC \ge 15\%$ ."

And at the end of **3.2.3.1 2**)

added mention of  $h\_icetop\_geoid\_uncrtn$  without changing the underlying meaning of the sentence, "average of  $h\_icetop\_geoid\_uncrtn = h\_uncrtn$  for IC  $\geq 15\%$ ."

2/27/2024 - In **1.2.4 1)** Added the sentence regarding lack of sea state bias in *h\_ice\_free*, "Note that because sea state bias, *bin\_ssbias*, is computed as an ocean segment average and not at the 10-m bin level, there is no correction for sea state bias in *h\_ice\_free*. This acceptable because sea state bias is small for ICESat-2 even in significant waves and wave amplitudes, which sea state bias depends on, are typically very small in the open water between ice floes."

2/27/2024 - To Table 3 added h icetop geoid avg uncrtn albm

2/27/2024 - In **3.2.4..2.2**, Removed calculation of *bias12rel07\_coefs* from Table 3 and text describing generation of the bias distribution with ice concentration to now read, "By outputting *h\_bias12rel07*, we will allow users to compute polynomial fits that will provide a monthly ice bias function."

2/28/2024 – In Table 3 added *h\_bias12rel07* and deleted *bias12rel07\_coefs*, Also eliminated mid-lat grids for *h\_icetop* variables

2/29/2024 - Corrected top of page 20 to

"For the polar grid simple averages, where *ice\_conc* is greater than or equal to 15%, we apply simple segment all-beam gridding to *h\_ice\_free*, *h\_atl07\_ice\_free*, and *h\_atl07\_inatl12oc* to produce *dot\_icefree\_avg\_albm*, *dot\_avginice\_07\_albm*, and *dot\_avginice\_7in12\_albm*."

And 1.2.4 and 3.2.3.1 simple average specifications to

"For the polar grid simple averages, where *ice\_conc* is greater than or equal to 15%, we also all-beam average *h\_ice\_free*,

h\_atl07\_ice\_free and h\_atl07\_inatl12oc as:

- 1) dot\_icefree\_avg\_albm
- 2) dot avginice 07 albm for h at 107 ice free, and
- 3) dot avginice 7in12 albm for h atl07 inatl12oc

We will also all-beam average the h\_ice\_free\_uncrtn, h\_atl07\_ice\_free\_uncrtn and h\_atl07\_inatl12oc\_uncrtn as dot\_icefree\_uncrtn\_albm, dot\_avginice\_07\_uncrtn\_albm and dot avginice 7in12 uncrtn albm, respectively."

3/5/2024 – removed from Table 3 a vestigial *h\_ice\_free\_avg\_albm* 3/12/2024 - In 3.2.4.2.2 improved the paragraph below describing *h\_bias12rel07* and added *h\_bias12rel07\_nsegs*, *h\_bias12rel07\_ttl*, and *h\_bias12rel07\_ttl\_nsegs*, Also added *h\_bias12rel07\_nsegs*, *h\_bias12rel07\_ttl\_nsegs*, *h\_bias12rel07\_ttl\_nsegs*, and *h\_bias12rel07\_tt* 

"However, for particular months we will arrive at corrections to *h* ice free to better match ATL07 DOT. For all the ATL12 ocean segments in each month and each bin to be gridded that have sea ice data, we will compute *h* bias12rel07 equal to the difference between h ice free and h atl07 ice free in 5% ice concentration bins, e.g., 15% to  $\leq 20\%$ ,  $\geq 20\%$  to  $\leq 25\%$ , ....  $\geq 95\%$  to  $\leq$ 100% with bin centers as bin lables. As noted above, for our test case during development these errors are at the 1-cm level and virtually constant with ice concentration (Fig. 2). We will also output the number of ocean segments that contribute to each ice concentration bin as h\_bias12rel07 nsegs. By outputting grid cell h bias12rel07 bias distributions versus ice concentration, we will allow users to compute polynomial fits that will provide a monthly ice bias function. Then, if necessary, corrections can be estimated to bring ATL19 DOT closer to ATL21 DOT on a grid cell by grid cell basis.

We will also compute *h\_bias12rel07\_ttl* equal to the aggregate of *h\_bias12rel07* over all grid cells in each Polar grid. We will output these and *h\_bias12rel07\_ttl\_nsegs*, the aggregate number of ocean segments that contribute to each *h\_bias12rel07\_ttl* as *h\_bias12rel07\_ttl nsegs*."

3/13/2024 – In Table 3 removed "Invalid" from specification for h\_bias12rel07, h\_bias12rel07\_nsegs, h\_bias12rel07\_ttl, and h\_bias12rel07\_ttl\_nsegs

4/2/2024 Change to 3.2.3.2 to perform the 3-Sigma edit only for ice concentration < 15%

We find that for reasons that we are investigating, ATL12 produces some ocean segment heights that are unrealistic compared to the geoid. For each 4-orbit ATL12 file, data from all six beams are concatenated. Means of dynamic ocean topography (DOT equal to h-geoid\_seg-bin\_ssbias) for ice concentration <15% are computed for each of the 18 ten-degree latitude bands for an ATL12 file. The latitude bands are centered on the 5° marks and do not overlap, i.e.  $\{90\text{S}^{\circ} \le \text{ATL}12 \text{ latitudes} \le 80^{\circ}\text{S}\}$ ,  $\{80^{\circ}\text{S} \le \text{ATL}12 \text{ latitudes} \le 70^{\circ}\text{S}\}$ , ...  $\{80^{\circ}\text{N} \le \text{ATL}12 \text{ latitudes} \le 90^{\circ}\text{N}\}$ ). The standard deviation,  $\sigma$ , of the DOT for ice concentration <15% from the entire ATL12 file is also computed, and DOTs for ice concentration <15% that are outside of  $\pm 3\sigma$  from the associated latitude-band mean, are removed.

4/2/2024 In 3.2.4.2.2 change the  $h\_bias12rel07$  ice concentration bin definition slightly to conform with ASAS so that bin limits are greater than or equal to the low concentration limit and less than the high concentration limit except also include concentrations equal to 100% in the 95% to 100% bin, i.e.:

 $h\_bias12rel07$  equal to the difference between  $h\_ice\_free$  and  $h\_atl07\_ice\_free$  in 5% ice concentration bins, e.g., concentration ≥5% to <10%, ≥10% to < 15%, ≥15% to < 20%, ... ... ≥90% to < 95%, ≥ 95% to ≤ 100% with bin centers as bin labels.

8/12/2024 In Section 1.1.4, changed tide model specification from "GOT4.8" to "FES2014b extrapolated"

10/26/2024 In section 1.2.4 edited for clarity paragraph for ice concentration greater than 70% to be

## IC > 70%

Also, if ice concentration is greater than 70% and **h\_atl07\_inatl12oc** exists, **h\_atl07\_inatl12oc** will be substituted for the open ocean DOT variable, **h-geoid\_seg-bin\_ssbias**, in the gridding process and the uncertainty in this value,

<ul><li>h_atl07_inatl12oc_uncrtn will be substituted for h_uncrtn as the DOT uncertainty in the gridding processes.</li></ul>	
10/27/2024 – Remove Section 3.2.4.2.3 "Averaging for Grid Cells in the Marginal Ice Zone (MIZ)" because there was not time to develop this product and removed <i>dot_avglw</i> from Table 3 of Outputs.	

# List of TBDs/TBRs

Item	Location	Summary	Ind./Org.	Due Date
No.				Date

## **Table of Contents**

Abstract	ii
CM Foreword	iii
Preface	iv
Review/Approval Page	v
Change History Log	vi
List of TBDs/TBRs	
List of Figures	
List of Tables	
1.0 Introduction and Background	
1.2 ATL19 Gridded Product	
1.2.1 ATL19 Grids	
1.2.2 The Basic Product	
1.2.3 All-beam and running 3-month averages	
1.2.4 Gridding DOT in Ice-covered Waters	
1.2.5 Elements for Optimal interpolation of DOT	
2.0 Gridded Ocean Product (ATL19/23 L3B)	7
2.1 Gridded DOT	
2.1.1 Grid Parameters	
3.0 Algorithm Implementation	я
3.1 Block Diagram for ATL19/23 Processing	8
3.2 Gridding DOT for ATL19/23	
3.2.1 The Grids	
3.2.2 Temporal Averaging	
3.2.3 Input to Gridding	
3.2.4 Gridding	
3.2.5 Gridding Output	29
3.3 Gridding DOT for ATL23	37
ACRONYMS	38
GLOSSARY	39
APPENDIX A: ICESat-2 Data Products	
APPENDIX B: Fitting a Plane to Spatially Distribute	
APPENDIX C: Hierarchy of ATL12 and ATL19/23 Va	
APPENDIX D: All-beam Average Equivalencies	
APPENDIX E: Optimal Interpolation of ICESat-2 Dyn	

# **List of Figures**

<u>Figure</u> Figure	1. ICESat-2 spacecraft and beam configuration (left) and footprints flying in
Figure	the forward direction
Figure	3. Block diagram for the ATL19 gridding procedure taking ATL12 ocean products as input. m, s, S, and K denote mean, standard deviation, skewness, and kurtosis respectively
Figure	4. Number of ocean segments found in each grid cell of the ¼° mid-latitude grid in August 20209
Figure	5. Number of ocean segments in August 2020 in each 25-km grid cell of the north polar stereographic grid (left) and the south polar stereographic grid (right). Color scale is number of ocean segments in a grid cell per month and x and y-axes are in 10 <sup>3</sup> km
Figure	6. Conceptual drawing of the sea-ice related variables from ATL12 that include ATL07-identified open water Bright leads in sea ic
Figure	7. Mid-latitude grid averages of DOT strong beams, Beam 1 (left) and Beam 2 (right), August 2020. Average DOT differences: beam2 – beam1 = 0.61 cm, beam3 – beam1 = 0.55 cm, beam2 – beam3 = -0.08 cm. The blank rectangle in the Central Pacific is the region of ocean–scans not gridded according to the pointing and orbit determination flag
Figure	8. Mid-latitude DOT gridded by simple "n-segment" all-beam averages (left) and degree-of-freedom weighted (dfw) all-beam averages (right) for August 2020. The ocean scan region in the Central Pacific is not gridded
Figure	9. Centered grid averages using 9-cells (3x3) to fit to the center of a center cell for 1-month, August 2020, (left) and 3-months, Jul-Aug-Sept. 2020, (right)29

# **List of Tables**

<u>Table</u>	<u>Page</u>
Table 1 Input to ATL19 from ATL12	.14
Table 2 Inter-beam biases OctNov. 2020	.19
Table 3 Output of ATL19	.30

## 1.0 INTRODUCTION AND BACKGROUND

This ATBD will cover the gridding of dynamic ocean topography and related variables from ICESat-2 ATL12 sea surface height (SSH).

## 1.1 Background: ATL03 and ATL12

The Ice, Cloud and land Elevation Satellite 2 (ICESat-2) is a photon-counting pulsed laser altimeter intended primarily to map the heights of the Earth's ice and snow-covered and vegetated surfaces. Its Advanced Topographic Laser System (ATLAS) projects 3 pairs of strong and weak beams pulsed at 10 kHz. For each beam, it measures the time of flight of individual photons to the Earth's surface and back. This range combined with precision pointing and orbit determination is used to measure the height of the surface along ground tracks numbered from left to right (gt1L, gt1R, gt2L, gt2R, gt3L, and gt3R) across the path of ICESat-2 (Fig. 1 right). The 6 beams are arranged in 2 rows of 3 with the weak beams forward when flying in the forward direction. The track assignments of the beams are as shown in Figure 1 (when during half the year ICESat-2 is flying backward the ground tracks remain numbered left to right but the beam assignments flip left to right). With the spacecraft yawed slightly to the left the weak and strong beam tracks of each pair are separated by only 90 m with the tracks of the strong-weak pairs separated 3 km across track. Each pulse of each beam illuminates a patch on the surface about 14-m across, and with the spacecraft moving at 7 km s<sup>-1</sup>, new patches are illuminated every 0.7 m, giving ICESat-2 unparalleled along track spatial resolution. The orbit of ICESat-2 extends to North and South 88° to capture the Polar Regions and repeats every 91 days.

Although ICESat-2 was not intended primarily as an ocean altimeter, its fine resolution and polar reach make it a uniquely exciting ocean instrument. Consequently, the ICESat-2 ATL12

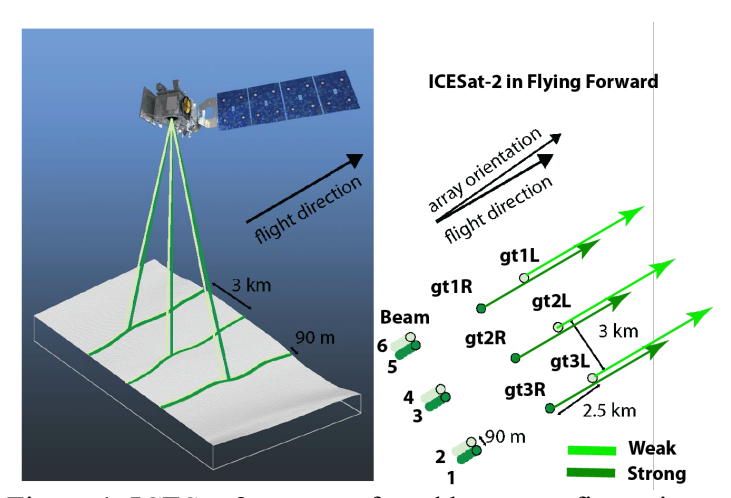


Figure 1. ICESat-2 spacecraft and beam configuration (left) and footprints flying in the forward direction.

along track ocean surface height product has been developed (Morison et al., 2019). It draws input data mainly from the ICESat-2 ATL03 Global Geolocated Photon heights product.

The ICESat-2 ATL03 [Neumann et al., 2021a, 2021b] provides the photon reflection height (referred to as photon height) of the ocean surface relative to the WGS84 ellipsoid for the downlinked data of each of the 6 beams. Originally, over the ice-free ocean and away from land only the strong beam data were downlinked to conserve downlink data volume, and weak beam data was only acquired over

the ocean when near land or over sea ice. Beginning in the summer of 2021, this limitation has been relaxed so that strong and weak beam data everywhere is downlinked from the satellite. The raw photon heights are corrected for atmospheric delay and standard geophysical corrections such as solid earth tide of common concern to all the higher-level ICESat-2 products (e.g., land ice, sea ice and vegetation). A statistical approach is used to assign a confidence rating to the likelihood of each photon height being a surface height.

The processing of the ATL03 photon heights to produce the ATL12 ocean surface height [Morison et al., 2019] first involves removing from the photon heights the expected high frequency variations due to tides from the FES2014b extrapolated model and short period atmospheric forcing with a Dynamic Atmospheric Correction (DAC) based on the 6-h AVISO MOG2D. To further reduce the height variability of the raw photon heights, the EGM2008 geoid in the mean tide system is subtracted, so that processing begins with photon heights expressed as dynamic ocean topography (DOT) dealiased for tides and short period atmospheric forcing. The processing system then accumulates histograms of these dealiased and geoid-referenced photon surface heights along each ground track over ocean segments long enough to acquire 8,000 surface-reflected photons or up to a maximum length of 7 km. Minimum ocean segment lengths are usually 3 or 4 km. To better exclude subsurface returns under the crests of waves, surface finding is actually done on the basis of histograms of the photon height anomalies relative to a running 11-point average of the photon heights deemed high confidence surface photons in ATL03. The histogram of these anomalies is then trimmed of noise photons in the high and low tails of the distribution. Once the surface photons are so identified, their actual heights are used in subsequent processing.

To account for the instrumental uncertainty in photon time of flight due mainly to uncertainty in the start time of the photon flights within each laser pulse, the instrument impulse response histogram derived from the downlinked Transmit Echo Pulse (TEP) is deconvolved from the received height histogram to yield a surface histogram.

The ATL12 main outputs are the mean and next three moments of the resulting histogram. The 10-m along-track bin averages of photon heights are computed and used to determine electromagnetic (EM) sea state bias (hereafter referred to as SSB) and wave harmonics projected on to the ground track direction. Uncertainty in the mean surface height is largely due to sampling the wave covered surface and is proportional to significant wave height (SWH) and inversely proportional to the square root of ocean segment length divided by the correlation length scale. For ATL12 Release 4 and beyond, the 10-m along-track averages are used to yield the track-projected wave harmonics, correlation scale, and degrees of freedom.

In addition to data from ICESat-2 ATL03, ATL12 pulls in data from outside sources such ocean depth from GEBCO and in Release 5, ice concentration from NSIDC.

## 1.2 ATL19 Gridded Product

The ATL19 gridded product is intended to provide users with a realization of the height of the ocean surface mapped over the world ocean in 1-month (and ultimately 3-month) averages. This

contrasts with the ATL12 ocean surface height, which is an along-track record of sea surface height and related variables, each file of which covers only four ICESat-2 orbits representing 6 hours. The primary ATL19 gridded product is dynamic ocean topography (DOT), which is sea surface height relative to the WGS84 ellipsoid minus the height of the EGM 2008, mean-tide geoid [Neumann et al., 2021b] relative to the WGS84 ellipsoid. The ATL12 processing mainly works with DOT to avoid the large variations associated with the geoid, but consistent with prior NASA planning ATL12 outputs ocean segment averages of the SSH and the geoid required to compute ocean segment-averages of DOT. We chose the primary output of ATL19 to be DOT (with the corresponding geoid as an ancillary variable to enable determination of SSH) because the variations in DOT represent familiar circulation patterns and because being much smaller than SSH variations, inter-beam biases and error stand out sharply in DOT.

## 1.2.1 ATL19 Grids

ATL19 uses 3 grids, North and South polar stereographic 25-km grids as well as an overlapping mid-latitude curvilinear ¼° latitude-longitude grid between 60°S and 60°N. The gridding is done individually for each beam on the ocean segments for each beam with average positions inside a grid cell.

## 1.2.2 The Basic Product

The basic product includes one-month simple averages and averages weighted by the estimated degrees of freedom for each beam ocean segment. Computing the individual beam averages provide a measure of relative biases among the six beams. The simple and degree-of-freedom weighted average grid or latitude-longitude positions of all the beam ocean segments in a grid cell are also output as are the simple and degree-of-freedom weighted averages of other key variables necessary to interpret DOT, such as the geoid and the sea state bias are also provided.

## 1.2.3 All-beam and running 3-month averages

The present release includes all-beam averages and planar fits over 9 cells to interpolate DOT to grid cell centers. ATL23 is based on three-month running averages of the ocean segment DOT which provides more complete filling of grid cells and better interpolation of DOT to the center of the grid cells. ATL23 grids are provided for each month using a sliding three-month window. The ATL23 file naming convention uses the first month in the file name, with ATL12 data from the two subsequent months forming each three-month ATL23.

## 1.2.4 Gridding DOT in Ice-covered Waters

DOT as provided by prior releases of ATL12/19/23 was biased by sea ice freeboard in ice covered oceans. With Release 4 and later releases of ATL19/23, we account for this with estimates of DOT in open water "bright" leads identified in ATL07 and incorporated into ATL12

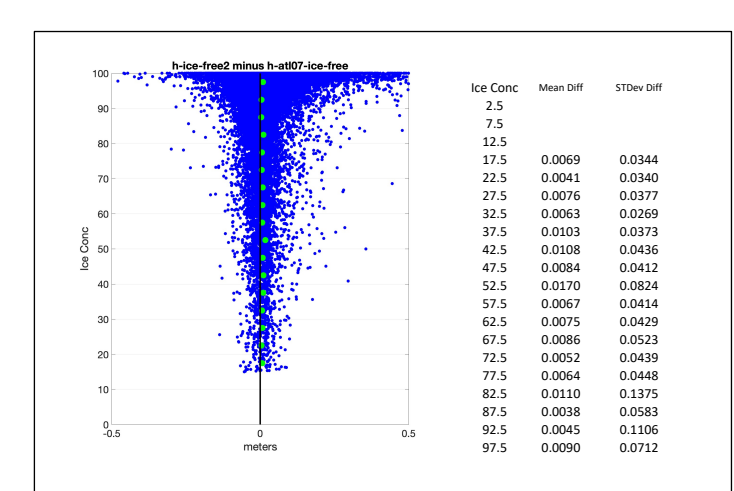


Figure 2. ATL12 v. ATL07 comparison, (left) h\_ice\_free-h\_atl07\_ice\_free versus ice concentration and (right) Table of h\_ice\_freeh\_atl07\_inatl12oc versus ice concentration.

as bright lead-qualified 10-m bins. In processing ATL12 Release 7 we synchronized with ATL07 to the degree that we can identify the 10-m bins that correspond to the ATL07 segments with ssh flag=1 indicative that these bright leads are suitable for sea surface height determination. We find that ATL12 DOT, *htvbin*, in 10-m bins, when it is corrected for first photon bias (fpb 10m), largely agrees with the corresponding ATL07 DOT with dynamic atmospheric correction as opposed to the dynamic IB correction. For each ATL12 ocean segment with corresponding ATL07, ATL12 computes: h ice free as the average DOT from ATL12 heights, htybinfpb 10m, in 10-m bins in common with

ssh\_flag qualified ATL07 sea ice segments, h\_atl07\_ice\_free as the average DOT from ATL07 in ssh\_flag=1 qualified sea ice segments with corresponding ATL12 10-m bins, and h\_atl07\_inatl12oc as the averaged DOT from all ATL07 ssh\_flag =1 qualified sea ice segments in an ATL12 ocean segment with or without corresponding ATL12 10-m bins. In testing we find h\_ice\_free agrees with h\_atl07\_ice\_free and h\_atl07\_inatl12oc to within 1 or 2 cm for ice concentrations less than 77.5% (Fig. 2). This indicates the basic surface finding used in ATL12 agrees with that used in ATL07. At high ice concentrations, h\_ice\_free is sometimes biased high. We believe this happens because leads are narrow relative to 10-m and laser pulses centered in the lead also pick up photon heights from the top of adjacent ice.

Consequently, in ATL19/23 for ocean segments with ice concentration, *ice\_conc*, greater than 15%, a variable referring to the height of the top of the sea ice surface relative to the geoid, *h\_icetop\_geoid*, will be set equal to *h-geoid\_seg-bin\_ssbias*.

## $15\% \le IC \le 70\%$

Also, for ice concentration from 15% to 70%, the value to be used for DOT in place of *h*-geoid\_seg will then be set to invalid unless:

1) h\_ice\_free exists, in which case h\_ice\_free will be substituted for the open ocean DOT variable, h-geoid\_seg-bin\_ssbias, in the gridding process and the uncertainty in h\_ice\_free, h\_ice\_free\_uncrtn, will be substituted for h\_uncrtn as the DOT uncertainty in the gridding processes. Note that because sea state bias, bin\_ssbias, is computed as an ocean segment average and not at the 10-m bin level, there is no correction for sea state bias in h\_ice\_free. This acceptable because sea state bias is small for ICESat-2 even in significant waves and

wave amplitudes, which sea state bias depends on, are typically very small in the open water between ice floes.

2) Or if h\_ice\_free does not exist (is invalid) but h\_atl07\_inatl12oc does exist, h\_atl07\_inatl12oc will be substituted for the open ocean DOT variable, h-geoid\_segbin\_ssbias, in the gridding process, and if h\_atl07\_inatl12oc\_uncrtn exists it will be substituted for h\_uncrtn as the DOT uncertainty in the gridding processes, or if h\_atl07\_inatl12oc\_uncrtn does not exist, a fixed empirical uncertainty, e.g., ± 5 cm, will be substituted for h\_uncrtn as the DOT uncertainty in the gridding processes.

## IC > 70%

Also, if ice concentration is greater than 70% and **h\_atl07\_inatl12oc** exists, **h\_atl07\_inatl12oc** will be substituted for the open ocean DOT variable, **h-geoid\_seg-bin\_ssbias**, in the gridding process and the uncertainty in this value, **h\_atl07\_inatl12oc\_uncrtn** will be substituted for **h\_uncrtn** as the DOT uncertainty in the gridding processes.

Note this change of variables to account for DOT in sea ice and can be performed on all the ATL12 data in a pass before going into the gridding or it can be performed as data is assigned to grid cells.

For the polar grid simple averages, where *ice\_conc* is greater than or equal to 15%, we also all-beam average *h ice free*, *h atl07 ice free* and *h atl07 inatl12oc* as:

- 1) dot\_icefree\_avg\_albm
- 2) dot avginice 07\_albm for h\_atl07\_ice\_free, and
- 3) dot avginice 7in12 albm for h atl07 inatl12oc

We will also all-beam average the <code>h\_ice\_free\_uncrtn</code>, <code>h\_atl07\_ice\_free\_uncrtn</code> and <code>h\_atl07\_inatl12oc\_uncrtn</code> as <code>dot\_icefree\_uncrtn\_albm</code>, <code>dot\_avginice\_07\_uncrtn\_albm</code> and <code>dot\_avginice\_7in12\_uncrtn\_albm</code>, respectively.

For the polar grids and IC  $\geq$  15%, we will compute and output  $h\_icetop\_avg\_allbm$  as the all-beam average of  $h\_icetop\_geoid$  (set equal to ATL12  $h\_geoid\_seg\_bin\_ssbias$  for IC  $\geq$  15%). This will be representing the top surface of the sea ice so that users may subtract gridded DOT to represent sea ice freeboard. The average uncertainty in  $h\_icetop\_avg\_uncrtn\_allbm$  will be computed as the all-beam average of  $h\_uncrtn$  for IC  $\geq$  15%.

## 1.2.5 Elements for Optimal interpolation of DOT

One-month gridded and even three-month gridded ICESat-2 data have unfilled grid cells. We want to provide the ATL19/23 user with as much information as possible for ICESat-2 to be optimally interpolated over a wide a range of regions and temporal resolutions as well as optimally interpolated global maps of DOT in ATL19/23. We think the 3-month moving averages that will be part of ATL23 are candidates for the background fields (*B* in Appendix E) underlying DOT anomalies to be interpolated at finer scales. ATL12 and ATL19/23 are unique

in providing degree-of-freedom and uncertainty estimates for ocean segment and gridded DOT, which provide measurement error values for each grid cell observation ( $\boldsymbol{D}$  in Appendix E).

## 2.0 GRIDDED OCEAN PRODUCT (ATL19/23 L3B)

## 2.1 Gridded DOT

ATL19, based on ATL12, contains gridded monthly estimates of DOT from all ICESat-2 tracks from the beginning to the end of each month. ATL23, similarly, contains gridded estimates spanning three-months, from the beginning of the first month to the end of the third month. Below 60°N and above 60°S, the data are mapped on the ¼°curvilinear latitude-longitude grid. In response to reviewer comments, these latitude limits will be increased in the future to 66°N and 66°S to match the region of TOPEX/Poseidon coverage. Above 60°N and below 60°S, the grid data are mapped onto a planimetric grid using the NSIDC Sea Ice Polar Stereographic grids (https://nsidc.org/data/polar-stereo/ps\_grids.html) with a grid spacing of 25 km. In the polar oceans the ATL10 sea ice products and ATL21 gridded sea ice products will eventually be reconciled with ATL12 and ATL19 data by methods TBD.

#### 2.1.1 Grid Parameters

## 2.1.1.1 DOT

With only ATL12 needed as input, the primary ATL19/23 will be grid cell averages of product dynamic ocean topography (DOT), the sea surface departure from the EGM2008 mean-tide geoid. These include simple arithmetic 1-month averages of DOT, degree-of-freedom-weighted averages and multi-cell, least-squares linear interpolations to grid cell centers. In addition to the mean, the product will include standard deviation, skewness, and kurtosis, propagated from 2<sup>nd</sup>, 3<sup>rd</sup>, and 4<sup>th</sup> moments from ATL12 ocean segments included in each grid cell.

The corresponding averages of position, geoid height, SSB, ocean depth, ice concentration, and other pertinent parameters from each segment will also be output. The mean SSH can be calculated as the mean DOT plus the weighted average geoid height.

## 2.1.1.2 Sea surface statistics histogram within grid

For each month, the aggregate histogram of photon heights expressed as DOT accumulated in the cell for all ocean segments in a grid cell will be output. The mean SSH can be calculated as the mean DOT plus the weighted average geoid height.

## 2.1.1.3 Wave statistics within grid

Estimates of SWH and SSB from the *a priori* estimation of sea state bias will also be grid-averaged with appropriate normalization for the number of surface photons in each segment.

#### 3.0 ALGORITHM IMPLEMENTATION

This section provides a more detailed description of the calculations of the ATL19 gridded products. It is meant to guide the derivation of both the development MATLAB code and the NASA ASAS computer code that will be used to produce ATL19. During development of the ASAS code, its output will be checked against the MATLAB code for selected ATL12 input data.

## 3.1 Block Diagram for ATL19/23 Processing

This product, based on Product ATL12/3A, contains gridded monthly estimates of DOT from all ICESat-2 tracks from the beginning to the end of each month. Below 60°N and above 60°S, the data are mapped on the ½°curvilinear latitude-longitude grid. In response to reviewer comments, these latitude limits will be increased in the future to 66°N and 66°S to match the region of TOPEX/Poseidon coverage. Above 60°N and below 60°S, the grid data are mapped onto a planimetric grid using the NSIDC Sea Ice Polar Stereographic grids (<a href="https://nsidc.org/data/polar-stereo/ps\_grids.html">https://nsidc.org/data/polar-stereo/ps\_grids.html</a>) with a grid spacing of 25 km.

ATL12 provides the histograms and first four moments of dynamic ocean topography over ocean segments up to 7-km long (DOT can be converted to SSH by adding ocean segment average geoid height, which is also output by ATL12). It also provides the number of photon

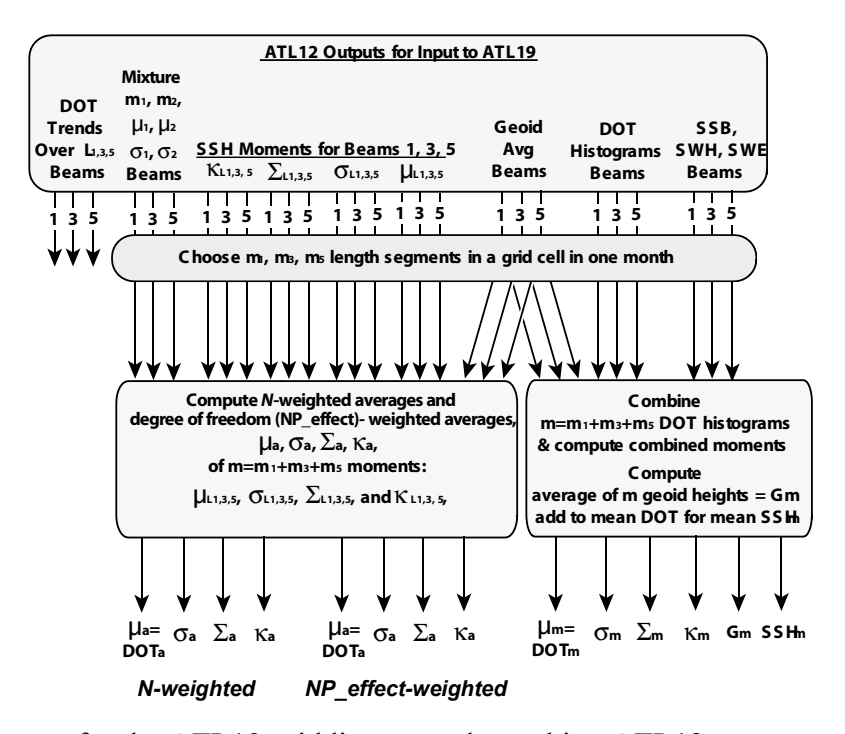


Figure 3. Block diagram for the ATL19 gridding procedure taking ATL12 ocean products as input.  $\mu$ ,  $\sigma$ ,  $\Sigma$ , and K denote mean, standard deviation, skewness, and kurtosis respectively.

heights, n photons, going into the moments and an effective degrees-of-freedom, NP effect,

based on the correlation length scale of surface heights. Using these, ATL19/23 will produce monthly aggregate histograms of surface heights and averages of the ocean segment moments weighted by both *n* photons and *h* uncrtn (Fig. 3).

## 3.2 Gridding DOT for ATL19/23

The ATL19/23 product includes gridded monthly estimates of dynamic ocean topography (DOT) taken from ATL12 ocean segment data. Ocean segments range in length roughly from 3 to a maximum 7 km dependent on photon rate. For ATL19/23 the ocean segment data are averaged in ¼° latitude-longitude or 25-km polar stereographic grid cells. Data from all six beams are used, both individually and averaged together from the beginning to the end of each month, prior to the summer of 2021 only strong beam data were downlinked and available over most of the ocean.

## 3.2.1 The Grids

The ICESat-2 data from ATL12 are averaged onto three grids, called mid-latitude, north-polar and south-polar. The ATL19/23 data file has groups with similar names containing the gridded data from each of those regions. It is important to note that when we do gridding of individual beams (or in ATLAS terminology: spots) it does not imply that the individual ground tracks, gt1l; gt1r; gt2l; gt2r; gt3l; gt3r, from ATL12 are averaged. This is avoided due to the fact that the ground track of a beam changes depending on the flight direction of the spacecraft (Fig. 1) For ATL19/23, strong beams are kept together over yaw flips. This is so that knowing average DOT differences across grid cells is small, we can use the individual beam gridded DOT values for calculating the bias between spots/beams.

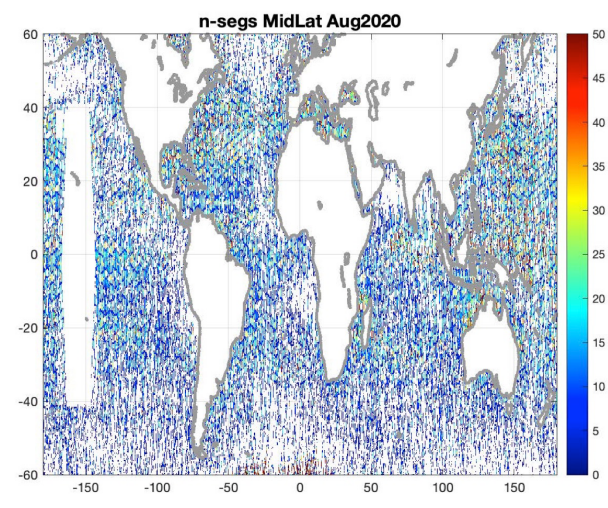


Figure 4. Number of ocean segments found in each grid cell of the ½° mid-latitude grid in August 2020.

The mid-latitude group contains ocean segment data mapped onto the curvilinear, ¼ ° latitude-longitude grid extending from 60°S to 60° (Fig. 4), to be expanded in future releases to 66°S to 66°N. The grid cells are centered on the odd 1/8<sup>th</sup> degree, with the latitude and longitude matrices defined in *gridcntr\_lat* and *gridcntr\_lon*, respectively. The matrix size of the gridded variables in the mid-latitude group is [480 x 1440].

As with the ATL20 product, ATL19/23 uses the North and South NSIDC Sea Ice Polar Stereographic grids (Fig. 5, https://nsidc.org/data/polarstereo/ps\_grids.html) to project data poleward of 60 degrees latitude. Both grids have a grid

spacing of 25 km, equivalent to 1/4 degree of latitude and are relative to the Hughes 1980

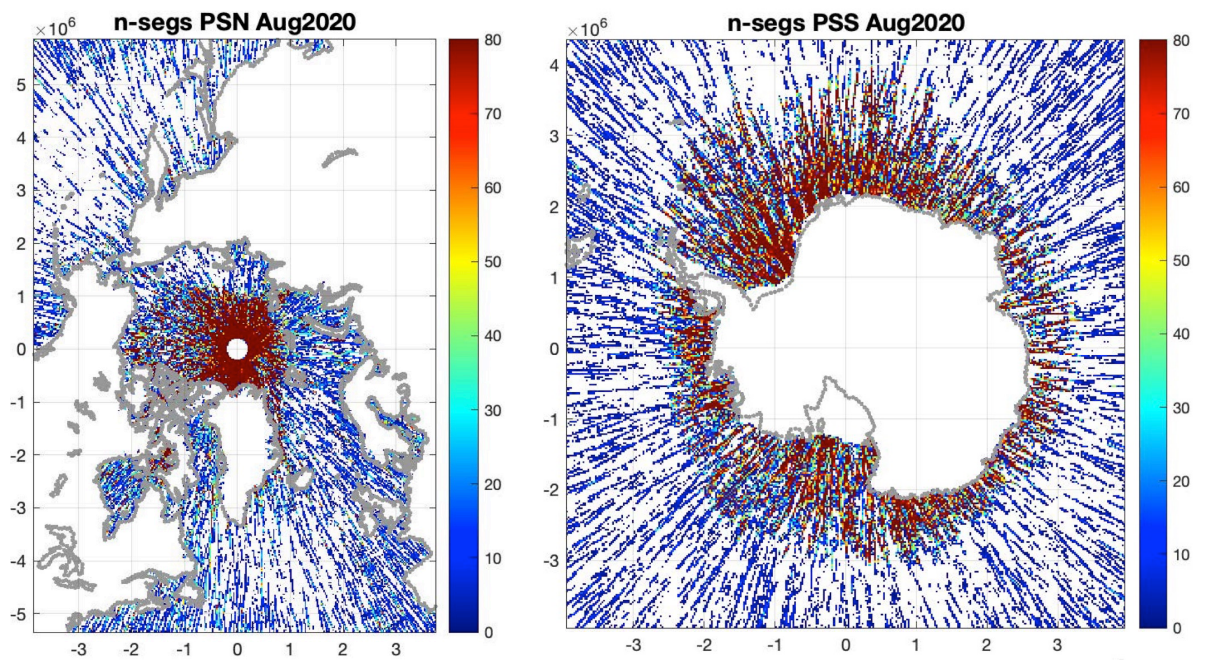


Figure 5. Number of ocean segments in August 2020 in each 25-km grid cell of the north polar stereographic grid (left) and the south polar stereographic grid (right). Color scale is number of ocean segments in a grid cell per month and x and y-axes are in 10<sup>3</sup> km.

Ellipsoid. The origins of these grids are at the poles and expressed in x and y distances from the poles. The North polar grid (<a href="https://epsg.io/3411">https://epsg.io/3411</a>) matrix is of size [448 x 304], with a true distance at 70°N and a central longitude along 45°E, with y positive along 135°E and x positive along 45°E The South polar grid (<a href="https://epsg.io/3412">https://epsg.io/3412</a>) matrix is of size [332 x 316], with a true distance at 70°S and a central longitude along 180°- 0°E with y positive along 0°E and x positive along 90°E. The ATL19/23 defined grid variables for the polar regions are <a href="mailto:ds\_grid\_x">ds\_grid\_y</a>. The north-polar and south-polar groups also contain *gridcntr\_lat* and *gridcntr\_lon*, similar to the mid-latitude group with latitude and longitude values converted from the x and y values in *ds\_grid\_x*, and *ds\_grid\_y*.

Major portions of each of these grids are not ocean, and the gridded sea surface height values for these grid cells will be set to a default invalid value.

## 3.2.2 Temporal Averaging

ATL19 includes monthly one-month averages and ATL23 include monthly, 3-month moving averages. The monthly 1-month data include aggregate histograms of DOT and averages of the ocean segment moments for data from all beams together and for each beam individually. The monthly gridded averages mid-latitude and polar grids do not produce averages for every grid cell, the sparseness of the averages being most pronounced at low latitudes. At the equator, the ICESat-2 orbits provide only one satellite pass per ½° of longitude over the 91-day repeat cycle.

Consequently, to provide better data coverage and allow a least squares linear interpolation of DOT to grid cell centers, ATL23 includes a least-squares planar fit among 9 (3X3) grid cells to grid cell centers. The goal is to provide data for every grid cell that is not perpetually under a heavy cloud cover.

## 3.2.3 Input to Gridding

Input to the ATL19 gridding process for each beam (ATLAS spot) includes the first four moments of sea surface height, mean SSH, h, variance of SSH, h var, skewness of SSH, h skewness, and kurtosis of SSH, h kurtosis, for each ocean segment from ATL12 (the moments in ATL12 are computed on DOT and the geoid is added to the mean to produce h). Simple averages and averages weighted by the degrees-of-freedom for each ocean segment are included. Prior to the February 8, 2022, version of this ATBD and in all ATL12, we have considered DOT strictly as surface height, h, minus the geoid. We have not applied a sea state bias correction, leaving that to the user. For the purposes of gridding, we have decided to apply the correction for sea state bias because for computing centered averages the coefficients for the planar fit of sea state bias would not necessarily be the same as those for the surface height minus the geoid. Appropriately weighted gridded sea state bias estimates will be included so that users can remove the sea state bias correction from gridded DOT. Thus, for the purpose of gridding, the gridded DOT is taken as sea surface height, h, minus the geoid height, geoid seg, and minus bin ssbias, i.e., DOT= h-geoid seg-bin ssbias. \* The gridded DOT variance, skewness, and kurtosis are derived from h var, h skewness, and h kurtosis respectively. Other geophysical variables gridded from the ATL12 include significant wave height, swh, sea state bias, bin ssbias and the aggregation of y histograms. (Note: ATL12 y is the histogram of DOT over an ocean segment minus meanoffit2, which is a preliminary mean DOT over the ocean segment.) Sea surface height uncertainty, h uncrtn, as well as the photon rate (photon rate) and the photon noise rate (photon noise rate) are also gridded. See Table 3 for complete list of ATL19 variables.

\*Reminder: In ATL12 processing to reduce variability due to the considerable non-oceanographic variation in the geoid, we work with DOT, the anomaly of photon heights about the geoid. ATL12 outputs sea surface height, h, relative to the WGS84 ellipsoid to be consistent with other ICESat output. For ATL12 output, ocean segment DOT is converted to mean sea surface height, h, by adding ocean segment mean geoid height, *geoid seg*, which is also output by ATL12.

For gridding purposes, ATL12 provides the number of photon heights, *n\_photons*, in each ocean segment used to determine the DOT moments. It also provides the effective degrees-of-freedom, *np\_effect*, which are based on the correlation length scale of surface heights and allow computing grid averages weighted by degrees of freedom. See Table 3 for complete list of ATL19 variables.

## 3.2.3.1 Variable Changes in Ice Covered Regions

DOT as provided by prior releases of ATL12/19/23 was biased by sea ice freeboard in ice covered oceans. With Release 4 and later releases of ATL19/23, we account for this with estimates of DOT in open water "bright" leads identified in ATL07 and incorporated into ATL12 as bright lead-qualified 10-m bins. In processing ATL12 Release 7 we have synchronized with ATL07 to the degree that we can identify the 10-m bins that correspond to the ATL07 segments

with *ssh\_flag*=1 indicative that these bright leads are suitable for sea surface height determination. We find that ATL12 DOT, *htybin*, in 10-m bins, when it is corrected for first photon bias, largely agrees with the corresponding ATL07 DOT with dynamic atmospheric correction as opposed to the dynamic IB correction. For each ATL12 ocean segment with corresponding ATL07, ATL12 computes: *h\_ice\_free* as the average DOT from ATL12 heights, *htybin*, in 10-m bins in common with *ssh\_flag*-qualified ATL07 sea ice segments (Fig. 6). It also computes *h\_atl07\_ice\_free* (Fig.6) as the average DOT from ATL07 in *ssh\_flag* qualified sea ice segments with corresponding ATL12 10-m bins and *h\_atl07\_inatl12oc* (Fig. 6) as the averaged DOT from all ATL07 *ssh\_flag*-qualified sea ice segments in an ATL12 ocean segment with or without corresponding ATL12 10-m bins. In testing we find *h\_ice\_free* agrees with *h\_atl07\_ice\_free* and *h\_atl07\_inatl12oc* to within 1 or 2 cm (Fig. 2) This suggests the basic surface finding used in ATL12 agrees with that used in ATL07.

Consequently, in ATL19/23 for ocean segments with ice concentration, *ice\_conc*, greater than 15%, a variable referring to the height of the top of the sea ice surface relative to the geoid, *h\_icetop\_geoid*, will be set equal to *h-geoid\_seg-bin\_ssbias*. The uncertainty in *h\_icetop\_geoid*,

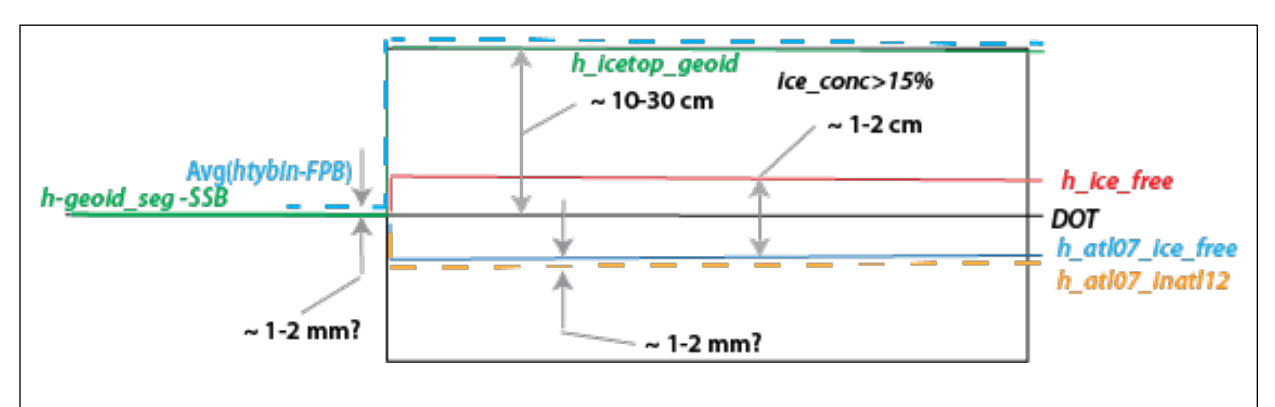


Figure 6. Conceptual drawing of the sea-ice related variables from ATL12 that include ATL07-identified open water Bright leads in sea ice.

h icetop geoid uncrtn, will be h uncrtn for IC  $\geq 15\%$ .

## $15\% \le IC \le 70\%$

Also, for ice concentration from 15% to 70%, the value to be used for DOT in place of *h*-geoid\_seg-bin\_ssbias will then be set to invalid unless:

- 1) h\_ice\_free exists, in which case h\_ice\_free will be substituted for the open ocean DOT variable, h-geoid\_seg-bin\_ssbias, in the gridding process and the uncertainty in h\_ice\_free, h\_ice\_free\_uncrtn, will be substituted for h\_uncrtn as the DOT uncertainty in the gridding processes.
- 2) Or if h\_ice\_free does not exist (is invalid) but h\_atl07\_inatl12oc does exist, h\_atl07\_inatl12oc will be substituted for the open ocean DOT variable, h-geoid\_segbin\_ssbias, in the gridding process, and if h\_atl07\_inatl12oc\_uncrtn exists it will be substituted for h\_uncrtn as the DOT uncertainty in the gridding processes, or if

 $h_atl07_inatl12oc_uncrtn$  does not exist, a fixed empirical uncertainty, e.g.,  $\pm$  5 cm, will be substituted for h uncrtn as the DOT uncertainty in the gridding processes.

#### IC > 70%

Also, for ice concentration greater than 70% and **h\_atl07\_inatl12oc** exists the value to be used for DOT in place of **h-geoid\_seg-bin\_ssbias** will then be set to t **h\_atl07\_inatl12oc** does exist, **h\_atl07\_inatl12oc** will be substituted for the open ocean DOT variable, **h-geoid\_seg-bin\_ssbias**, in the gridding process and the uncertainty in this value, **h\_atl07\_inatl12oc\_uncrtn** will be substituted for **h uncrtn** as the DOT uncertainty in the gridding processes.

Note this change of variables to account for DOT in sea ice can be performed on all the ATL12 data in a pass before going into the gridding or it can be performed as data is assigned to grid cells but the latter process would likely have to be repeated for each type of gridding.

For the polar grid simple averages, where *ice\_conc* is greater than or equal to 15%, we also all-beam average *h* atl07 ice free and *h* atl07 inatl12oc as:

- 1) dot icefree avg albm
- 2) dot\_avginice\_07\_albm for h\_atl07\_ice\_free, and
- 3) dot avginice 7in12 albm for h atl07 inatl12oc

We will also all-beam average the h\_ice\_free\_uncrtn, h\_atl07\_ice\_free\_uncrtn and h\_atl07\_inatl12oc\_uncrtn as dot\_icefree\_uncrtn\_albm, dot\_avginice\_07\_uncrtn\_albm and dot\_avginice\_7in12\_uncrtn\_albm, respectively.

For the polar grids and IC  $\geq$  15%, we will compute and output  $h\_icetop\_avg\_allbm$  as the allbeam average of  $h\_icetop\_geoid$  (set equal to ATL12 h-geoid\\_seg-bin\\_ssbias for IC  $\geq$  15%). This will be representing the top surface of the sea ice so that users may subtract gridded DOT to represent sea ice freeboard. The average uncertainty in  $h\_icetop\_avg\_uncrtn\_allbm$  will be computed as the all-beam average of h icetop geoid uncrtn = h uncrtn for IC  $\geq$  15%.

### 3.2.3.2 Pre-grid Filtering – Along-Track

The ATL12 ocean segment data going into ATL19/23 are already filtered for depths greater than 10-m and for pointing and orbit determinations outside of nominal conditions (ATL03 podppd flag = 0, nominal, or 4, nominal calibration maneuver). Ocean segment averages of depth, depth\_seg, and the highest of the podppd\_flag used in an ocean segment, podppd\_flag\_seg, are included in ATL12 output. ATL19 gridded averages of these quantities are computed as discussed below and in Table 3.

We find that for reasons that we are investigating, ATL12 produces some ocean segment heights that are unrealistic compared to the geoid. For each 4-orbit ATL12 file, data from all six beams are concatenated. Means of dynamic ocean topography (DOT equal to *h-geoid\_seg-bin\_ssbias*) for ice concentration <15% are computed for each of the 18 ten-degree latitude bands for an ATL12 file. The latitude bands are centered on the 5° marks and do not overlap, i.e. {90S° <= ATL12 latitudes < 80°S},

 $\{80^{\circ}\text{S} \le \text{ATL12 latitudes} \le 70^{\circ}\text{S}\}, \dots \{80^{\circ}\text{N} \le \text{ATL12 latitudes} \le 90^{\circ}\text{N}\})$ . The standard deviation,  $\sigma$ , of the DOT for ice concentration  $\le 15\%$  from the entire ATL12 file is also computed, and DOTs for ice concentration  $\le 15\%$  that are outside of  $\pm 3\sigma$  from the associated latitude-band mean, are removed.

### Table 1 Inputs to Ocean Gridded Products from ATL12 (See Table 6 in ATL12 ATBD for all ATL12 Outputs)

<b>Product Label</b>	Units	Description	Symbol
ds_y_bincenters	meters	Bin centers for y probability density function -15 to +15, by 1cm bins	ds_y_bincenters
gtx/ssh_segments/			
latitude	degrees	Mean latitude of surface photons in segment	lat_seg
longitude	degrees	Mean longitude of surface photons in segment	lon_seg
gtx/ssh_segments/ heights			
h	meters	Mean sea surface height relative to the WGS84 ellipsoid	SSH
h_var	meters <sup>2</sup>	Variance of best fit probability density function (meters <sup>2</sup> )	SSHvar
h_skewness		Skewness of photon sea surface height histogram	SSHskew
h_kurtosis		Excess kurtosis of sea surface height histogram	SSHkurt
h_ATL07_ice_free	m	Average DOT from ATL07 in ssh_flag=1 qualified sea ice segments with corresponding ATL12 10-m bins	h_atl07_ice_free
h_atl07_inatl12oc	m	Averaged DOT from all ATL07 in ssh_flag =1 qualified sea ice segments in an ATL12 ocean segment with or without corresponding ATL12 10-m bins	h_atl07_inatl12oc
h_ice_free	m	Average DOT from ATL12 heights, htybin, in 10-m bins in common with ssh_flag qualified ATL07 sea ice segments	h_ice_free
h_ice_free_uncrtn	meters	Uncertainty in h_ice_free	h_ice_free_uncrtn
meanoffit2	meters	Mean of linear fit removed from surface photon height expressed as DOT during surface finding	meanoffit2
у	m <sup>-1</sup>	Probability density function of photon surface height	Y

length_seg	meters	Length of segment (m)	length_seg
binsize	meters	Bin size for Y and sshx	Binsize
bin_ssbias	meters	Ocean segment sea state bias estimated from the correlation of photon return rate with along-track 10-m bin averaged surface height.	binSSBias
swh	meters	Significant wave height estimated as 4 times the standard deviation of along-track 10-m bin averaged surface height	SWH
xbin	meters	Center of 1 x 710 element array of 10-m bins. Note this may be included as a data description or other static array equal to [5, 15, 25, 35 7095 m]	Xbin
xbind	meters	1 x 710 element array of potential 10- m bin averages of along-track distance	Xbind
h_uncrtn	meters	Uncertainty in the mean sea surface height over an ocean segment	h_uncrtn
np_effect		Effective degrees of freedom of the average sea surface height for the ocean segment	NP_effect
l_scale		Correlation length scale expressed as a number of 10-m bins	Lscale
nbin10		Number of 10-m bins in an ocean segment	Nbin10
gtx/ssh_segments/s tats			
n_photons		Number of surface photons found for the segment	n_photon
n_ttl_photon		Total number of photons in the downlink band for the segment	n_ttl_photon
depth_ocn_seg	meters	The average of depth ocean of geosegments used in the ocean segment.	depth_ocn_seg
geoid_seg	meters	Ocean segment average of geoid height above the WGS – 84 reference ellipsoid (range -107 to 86 m)	geoid_seg
ice_conc		Ocean-segment average ice concentration per ATL12 ATBD Rel. 5 and greater	ice_conc

ice_conc_12icefree bins	ATL12 ocean-segment ice concentration based on the square of the complement of the fraction of 10-m bins classified as bright leads per ATL12 ATBD Rel. 7	ice_conc_12icefree bins
podppd_flag_seg	The higher of podppd_flag (0, nominal, or 4, nominal calibration maneuver) used in the ocean segment	podppd_flag
surf_type_prcnt	The percentages of each <i>surf_ty</i> pe of the photons in the ocean segment as a 5-element variable with each element corresponding to the percentage of photons coming from positions under each of the 5 surface masks. Due to mask overlaps, photons can originate from more than one mask type, and the 5 surface type percentages can total more than 100%.	surf_type_prcnt

### 3.2.4 Gridding

The ATL19 gridding process involves three general steps: binning, averaging, and interpolation to grid cell center. There are two averaging methods; simple averaging, and averaging weighted by the number of degrees of freedom of the ocean segment data. Data interpolated to grid cell center are also included in the ATL19 data product.

### 3.2.4.1 **Binning**

Consider one month of ATL12 concatenated data for each beam. Using the latitude and longitude from ATL12, *lat\_seg*, and *lon\_seg*, find the data that fall within a grid cell. For the polar grids, first convert the latitude and longitude to the appropriate polar stereographic coordinates *x\_seg* and *y\_seg* using libraries located at:

https://nsidc.org/data/polar-stereo/tools\_geo\_pixel.html with coordinate transforms for lat, lon to x, y and x, y to lat, lon also given in Appendix D. The appropriate grid bin containing each ocean segment can then be identified based on x\_seg and y\_seg and the x and y boundaries of the grid cells. Once the correct bin is identified, the data corresponding to Table 1 for that ocean segment is accumulated. This will result in each grid cell having a collection of the data from all n\_segs ocean segments contained in the grid cell for each beam (beam\_1, beam\_2, etc.).

Once the ocean segments appropriate to each bin are identified, compute  $n\_ph\_srfc$ , the sum of the number of surface reflected photons,  $n\_photons$ , for all ocean segments in the grid cell. Also compute  $n\_phs\_ttl$  as the grid cell-total of all photons in the downlink bands,  $n\_ttl\_photon$ . Compute dof equal to the sum of all the  $NP\_effect$  in the bin. Compute the total length of all ocean segments in the bin, length sum, as the sum of length seg. Also output the

number of segments in the bin, *n\_segs*. Additionally, compute the grid cell-aggregate photon rate, *r\_srfc*, equal to *n\_ph\_sfc* divided by the total length of segments in the bin, *length\_sum*. Finally, compute the grid cell noise rate, *r\_noise*, equal to (*n\_phs\_ttl* minus *n\_ph\_srfc*) divided by *length sum*.

### 3.2.4.2 Individual Beam Averaging

### 3.2.4.2.1 Averaging over n\_segs Segments

For each grid cell and each beam with the accumulated data of *n\_segs* ocean segments, compute outputs:

dot\_avg, lat\_avg, lon\_avg, ssb\_avg, geoid\_avg, depth\_avg, ice\_conc, and surf\_prcnt\_avg as simple averages of:

SSH-geoid\_seg, lat\_seg, lon\_seg, bin\_ssbias, geoid\_seg, depth\_ocn\_seg, ice\_conc, and surf type prcnt.

(In a related calculation, *length\_sum* will be computed as the sum of single beam ocean segment lengths, *length\_seg*, and *length\_sum\_albm* will be computed as the sum of all beam ocean segment lengths.)

Simple average is defined by the sum of the *n\_segs* ocean segment values of these variables divided by *n\_segs*. See Figure 7 for the August 2020 strong Beam-1 (Fig. 7 left) and strong Beam-3 (Fig. 7 right) "*n-segs*" averages, from our Matlab developmental code.

To compute the bin average standard deviation, *dot\_sigma\_avg*, of DOT variability over ocean segments, sum *SSHvar*, divide by *n\_segs*, and take the square root to establish the average standard deviation. Note that this and the other average moments do not include the ocean-segment-to-ocean-segment variability within the cell. This is likely much smaller than the variability due to sea state, but in future releases we plan to distinguish the ocean-segment-to-ocean-segment variability where adequate ocean segments are included by a TBD method.

Similarly, to compute the bin average significant wave height,  $SWH_avg$ , sum  $(SWH)^2$ , divide by n segs, and take the square root to establish the average significant wave height.

To compute the bin average skewness,  $dot_skew_avg$ , of DOT, sum SSHskew x  $(SSHvar)^{3/2}$ , divide by  $n_segs$ , and divide by  $dot_sigma_avg^3$  to establish the average skewness.

To compute the bin average excess kurtosis,  $dot_kurt_avg$ , of DOT, sum (SSHkurt+3) x (SSHvar)<sup>2</sup>, divide by  $n_segs$ , and divide by  $dot_sigma_avg^4$ . Subtract 3 to establish the average excess kurtosis.

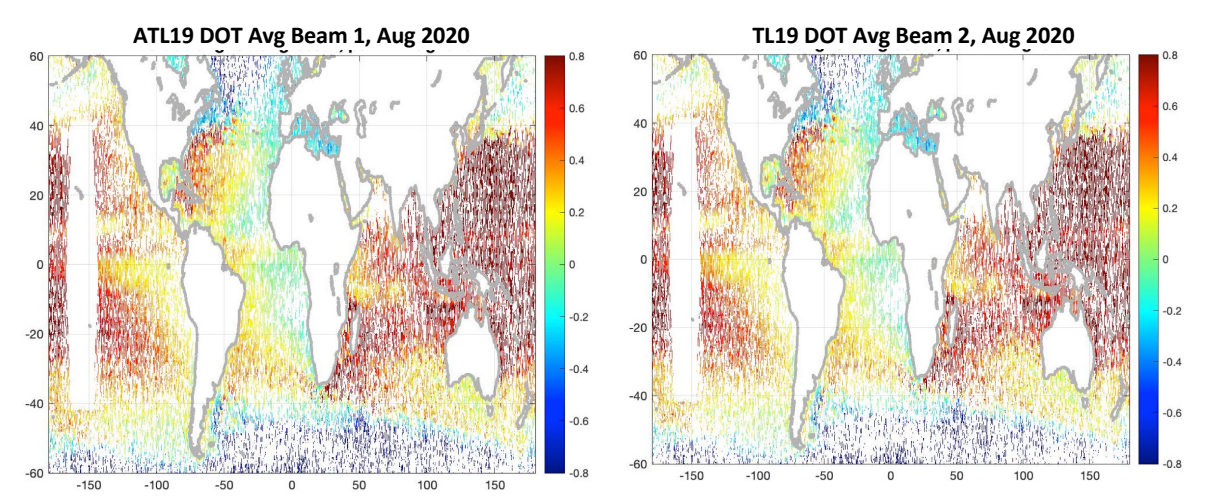


Figure 7. Mid-latitude grid averages of DOT strong beams, Beam 1 (left) and Beam 2 (right), August 2020. Average DOT differences: beam2 – beam1 = 0.61 cm, beam3 – beam1 = 0.55 cm, beam2 – beam3 = -0.08 cm. The blank rectangle in the Central Pacific is the region of ocean—scans not gridded according to the pointing and orbit determination flag.

To compute the uncertainty, *dot\_avg\_uncrtn*, in gridded DOT, *dot\_avg*, divide *dot\_sigma\_avg* by the square root of *dof* to establish the uncertainty in the degree-of-freedom weighted DOT. As with the higher moments, this is the uncertainty due to sea state and does not include the ocean-segment-to-ocean-segment variability within the cell. In future releases we plan to estimate the ocean-segment-to-ocean-segment uncertainty where adequate ocean segments are included by a TBD method.

To compute the bin aggregate probability density function (PDF), *dot\_hist*, of DOT, we first must convert each *Y* PDF from ATL12 to a PDF of DOT by adding *meanoffit2* to the x-axis of *Y*, *ds\_y\_bincenters* and then interpolating the result to an intermediate PDF, *Yintermediate*, evaluated at the original *ds\_y\_bincenters*. (Note: In ATL19 Release 1, meanoffit2 was inadvertently not added so the aggregate histograms only reflect the aggregate wave environment with mean near zero.) The aggregate probability PDF, *dot\_hist*, of DOT will equal the sum *Yintermediate x n\_photons* in each histogram bin of all *Yintermediate* divided by the total, *n\_photons\_gridttl*, of all *n\_photons. dot\_hist* extends over bins centered *ds\_hist\_bincenters* that are the same as *ds\_y\_bincenters*, i.e., ±15 m.

Note that in the implementation of Release 2 of ATL19, we found that including *dot\_hist* for each individual, beam each grid cell, and 6001 histogram bins used an excessive amount of storage necessitating the computation of *dot\_hist* only as an aggregate for all beams termed *dot\_hist\_albm*.

No Ocean Scans	Beam 1	Beam 2	Beam 3	Beam 4	Beam 5	Beam 6
Beam 1		0.0066	0.0066	0.0021	0.0066	-0.0089
Beam 2	-0.0066		-0.0024	-0.0017	0.0024	-0.0107
Beam 3	-0.0066	0.0024		-0.0001	-0.0001	-0.0116
Beam 4	-0.0021	0.0017	0.0001		0.0041	-0.0096
Beam 5	-0.0066	-0.0024	0.0001	-0.0041		-0.0152
Beam 6	0.0089	0.0107	0.0116	0.0096	0.0152	

Table 2: Mid-Latitude Inter-Beam Biases, Oct. & Nov. 2020

### 3.2.4.2.2 Averaging for Grid Cells Where Sea Ice is Present

As noted in Sections 1.2.4 and 3.2.3.1, ATL12 Release 7 comes with new parameters,  $h\_ice\_free$ ,  $h\_atl07\_ice\_free$ , and  $h\_atl07\_inatl12oc$  describing DOT in ice covered waters as well as uncertainties in these DOTs,  $h\_ice\_free\_uncrtn$ ,  $h\_atl07\_ice\_free\_uncrtn$ , and  $h\_atl07\_inatl12oc\_uncrtn$ .

For ice-covered waters, defined as ice concentration  $\geq 15\%$  and ice concentration  $\leq 70\%$ , the sea ice editing steps in Section 3.2.3.1 replace h-geoid\_seg-bin\_ssbias, the open water DOT, with h\_ice\_free, or h\_atl07\_inatl12oc if h\_ice\_free is invalid. Simultaneously, the uncertainty, h\_uncrtn, will be replaced with h\_ice\_free\_uncrtn, or h\_atl07\_inatl12oc\_uncrtn if h\_ice\_free is invalid.

For ice concentration >70%, the sea ice editing steps in Section 3.2.3.1 replace **h-geoid\_seg-bin\_ssbias**, the open water DOT, with **h\_atl07\_inatl12oc**. Simultaneously, the uncertainty, **h\_uncrtn**, will be replaced with **h\_atl07\_inatl12oc\_uncrtn**.

Thus, the gridding procedures from prior versions of ATL19/23 can be used without modification and the grids of DOT will truly represent the water surface in ice-covered waters.

However, this release also adds 3 sea ice DOT variables, h\_ice\_free, h\_atl07\_ice\_free, and h\_atl07\_inatl12oc along with their uncertainties, h\_ice\_free\_uncrtn, h\_atl07\_ice\_free\_uncrtn, and h atl07 inatl12oc uncrtn, to be grid-averaged in the simple all-beam method.

For ice concentration  $\geq 15\%$ , we also grid average a measure of the top surface of ice and water,  $h\_icetop\_geoid$  (Fig. 6), which in the sea ice editing steps is taken equal to  $h\_geoid\_seg\_bin$  ssbias, which alternatively is DOT in open waters.

For the polar grid simple averages, where *ice\_conc* is greater than or equal to 15%, we apply simple segment all-beam gridding to *h\_ice\_free*, *h\_atl07\_ice\_free*, and *h\_atl07\_inatl12oc* to produce *dot\_icefree\_avg\_albm*, *dot\_avginice\_07\_albm*, and *dot\_avginice\_7in12\_albm*.

Critical Note: In ice covered waters where we substitute h\_ice\_free or h\_atl07\_inatl12oc for h-geoid\_seg-bin\_ssbias, we will also substitute their uncertainties h\_ice\_free\_uncrtn or h\_atl07\_inatl12oc\_uncrtn, for the uncertainty in h, h\_uncrtn. This will be critically important in all the averaging schemes that weight by uncertainty, e.g., dot dfw and dot\_dfw9.

Further, for IC  $\geq$  15% we apply simple segment all-beam gridding to  $h\_icetop\_geoid$  as representing the top surface of the sea ice to produce  $h\_icetop\_geoid\_avg\_albm$  so that users may subtract gridded respective gridded DOT to represent sea ice freeboard. We also compute and output the uncertainty in the ice-top height,  $h\_icetop\_geoid\_avg\_uncrtn\_albm$ , as the all-bean average of  $h\_uncrtn$  where IC $\geq$  15%.

In global comparisons of 146 ATL12 files over different seasons, we find the average differences between *h\_ice\_free* and *h\_atl07\_ice\_free* are on the order of 1 cm with standard deviations less than 12 cm at the highest high ice concentrations and about 3 cm at low concentrations (Fig. 2) indicating good basic agreement of the surface finding in ATL12 and ATL07. We want the gridded averages of DOT in the ice to match gridded averages of *h-geoid\_seg-bin\_ssbias* at the ice edge where ice concentrations are low and the gradients of gridded DOT should be consistent with ATL07 DOT e.g., *h\_atl07\_ice\_free*, and *h\_atl07\_inatl12oc* in the pack ice where ice concentrations are greater. Because the average in open water of *htybin - bin\_ssbias* in open water nearly matches *h-geoid\_seg-bin\_ssbias* (Fig. 6), we assume the average DOT in the ice, incorporating *h\_ice\_free* based on bright lead-qualified *htybin* should match *h-geoid\_seg* at the ice edge. Further, the test results in Figure 2 suggest agreement is good with ATL07 for all ice concentrations.

However, for particular months we will arrive at corrections to  $h\_ice\_free$  to better match ATL07 DOT. For all the ATL12 ocean segments in each month and each bin to be gridded that have sea ice data, we will compute  $h\_bias12rel07$  equal to the difference between  $h\_ice\_free$  and  $h\_atl07\_ice\_free$  in 5% ice concentration bins, e.g., concentration  $\geq$ 5% to <10%,  $\geq$ 10% to <15%,  $\geq$ 15% to <20%, ... ...  $\geq$ 90% to <95%,  $\geq$ 95% to  $\leq$ 100% with bin centers as bin labels. As noted above, for our test case during development these errors are at the 1-cm level and virtually constant with ice concentration (Fig. 2). We will also output the number of ocean segments that contribute to each ice concentration bin as  $h\_bias12rel07\_nsegs$ . By outputting grid cell  $h\_bias12rel07$  bias distributions versus ice concentration, we will allow users to compute polynomial fits that will provide a monthly ice bias function. Then, if necessary, corrections can be estimated to bring ATL19 DOT closer to ATL21 DOT on a grid cell by grid cell basis.

We will also compute  $h\_bias12rel07\_ttl$  equal to the aggregate of  $h\_bias12rel07$  over all grid cells in each Polar grid. We will output these and  $h\_bias12rel07\_ttl\_nsegs$ , the aggregate number of ocean segments that contribute to each  $h\_bias12rel07\_ttl$  as  $h\_bias12rel07\_ttl\_nsegs$ .

### 3.2.4.2.3 Averaging Weighted by Degrees-of-Freedom-Uncertainty

To account for the different uncertainties in linear variables (e.g., DOT) the averaging is as in 5.6.4.2 except the variables are weighted by the inverse square of the uncertainty. Because uncertainty is equal to the standard deviation of height divided by the square root of degrees-of-freedom, weights equal to the inverse square of uncertainty are equal to degrees-of-freedom divided by wave induced height variance. In earlier versions of this ATBD, we weighted by degrees of freedom alone, but weighting by the inverse square of uncertainty equal to degrees-of-freedom over variance results in averages with the minimum uncertainty [citation needed]. These degree-of-freedom-uncertainty weighted averages will be different from simple averages in important ways for cases where different beams in a cell measure over different sea states and have different sea state induced DOT uncertainty. DOT measured under calm conditions will be more certain and receive greater weight than DOT measured over a large significant wave heights. Also, DOT measured over short wavelength waves will have more degrees-of-freedom, lower uncertainty, and receive greater weight than DOT measured over long waves with the same SWH.

For each grid cell and each beam with the accumulated data of *n\_segs* ocean segments compute outputs

dot\_dfw, lat\_dfw, lon\_dfw, ssb\_dfw, geoid\_dfw, and depth\_dfw as degree-of-freedom-uncertainty weighted averages of:

SSH-geoid\_seg, lat seg, lon seg, bin ssbias, geoid\_seg, and depth ocn seg.

Similarly, degree-of-freedom-uncertainty weighted averages *lat\_dfw9*, *lon\_dfw9*, and *dot\_dfw9* of *lat\_seg*, *lon\_seg*, and *h-geoid\_seg-bin\_SSbias* over the center cell and eight surrounding cells will be needed for computing centered dfw averages (Section 3.2.4.4.2).

Degree-of-freedom-uncertainty weighted averages are found by first taking the sum of the  $n\_segs$  ocean segment values multiplied by a weighting factor, Wi, equal to the inverse of their uncertainties squared  $Wi=(1/h\_uncrtn)^2$ . (Note: In ice covered waters,  $15\% \le ice\_conc \le 70\%$ , where we substitute  $h\_ice\_free$  for  $h\_geoid\_seg\_bin\_ssbias$ , we will also substitute the uncertainty in  $h\_ice\_free$ ,  $h\_ice\_free\_uncrtn$ , for the uncertainty in  $h\_uncrtn$ . Where  $ice\_conc > 70\%$ , we substitute  $h\_atl07\_inatl12oc$  for  $h\_geoid\_seg\_bin\_ssbias$ , and we will also substitute the uncertainty in  $h\_atl07\_inatl12oc$ ,  $h\_atl07\_inatl12oc\_uncrtn$ , for the uncertainty in  $h\_uncrtn$ . This will be critically important in the averaging schemes weighted by uncertainty for  $dot\_dfw$  and companion dfw-averaged variables). Doing so effectively deemphasizes ocean segments with low degrees of freedom or high wave induced ocean segment height variance and tend to minimize the uncertainty of the resulting average value. Then the sum is divided by the sum of the Wi to normalize the result and produce the degree-of-freedom-uncertainty weighted averages.

To compute the bin degree-of-freedom-uncertainty weighted average standard deviation of DOT, *dot\_sigma\_dfw*, of DOT, sum *SSHvar* multiplied by *Wi*. Then divide by the sum of the *Wi* and take the square root to establish the degree-of-freedom-uncertainty weighted standard deviation of DOT. Note that this and the other average moments do not include the ocean-

segment-to-ocean-segment variability within the cell. This is likely much smaller than the variability due to sea state, but in future releases we plan to distinguish the ocean-segment-to-ocean-segment variability where adequate ocean segments are included by a TBD method.

Similarly, to compute the bin degree-of-freedom-uncertainty weighted average significant wave height,  $SWH\_dfw$ , sum  $(SWH)^2$  multiplied by Wi. Then divide by the sum of the Wi and take the square root to establish the degree-of-freedom-uncertainty weighted average significant wave height.

To compute the bin degree-of-freedom weighted average skewness,  $dot_skew_dfw$ , of DOT, sum  $SSHskew \times (SSHvar)^{3/2}$ , multiplied by Wi. Then divide by the sum of the Wi and take the square root to establish the degree-of-freedom weighted and divide again by  $dot_sigma_dfw^3$  to establish the degree-of-freedom weighted skewness.

To compute the bin degree-of-freedom weighted average excess kurtosis,  $dot\_kurt\_dfw$ , of DOT, sum (SSHkurt+3) x (SSHvar)<sup>2</sup> multiplied by Wi. Then divide by the sum of the Wi and take the square root to establish the degree-of-freedom weighted and divide again by  $dot sigma dfw^4$ . Subtract 3 to establish the degree-of-freedom weighted excess kurtosis.

To compute the uncertainty, dot\_dfw\_uncrtn, in gridded DOT, dot\_dfw, divide dot\_sigma\_dfw by the square root of dof to establish the uncertainty in the degree-of-freedom-uncertainty weighted DOT. This as the ratio of dot\_sigma\_dfw to the square root of dof is not the not the same as the weighted average of individual ocean segment uncertainties, h\_uncrtn, but will probably be similar and is provided for comparison purposes. It like h\_uncrtn, does not include the ocean-segment-to-ocean-segment variability within the cell. In future releases we plan to estimate the ocean-segment-to-ocean-segment uncertainty where adequate ocean segments are included by a TBD method.

#### 3.2.4.2.4 Inter-Beam Biases

The procedures of section 3.2.4.2 will be performed independently for each beam, if for no other reason than a particular satellite pass may have ground tracks in adjacent pairs of cells. Furthermore, comparing the gridded product for the individual beams will disclose instrumental biases. For example, for August 2020, biases between the strong beams were significantly less than a centimeter (Figure 7), and Table 2 shows that the mid-latitude grid average inter-beam biases for October-November 2020 were mostly less than a centimeter. In the future inter-beam biases can be monitored with gridded single-beam averages and accounted for by a TBD method in a gridded product that combines all the beams.

### 3.2.4.3 All-beam Averages

We want all-beam quantities for each grid cell to achieve grid cell averages with maximum degrees of freedom and minimum uncertainty. Figure 8 shows DOT gridded by our developmental code in the mid-latitude grid by simple averaging (left) and degree-of- freedom weighted averaging (right).

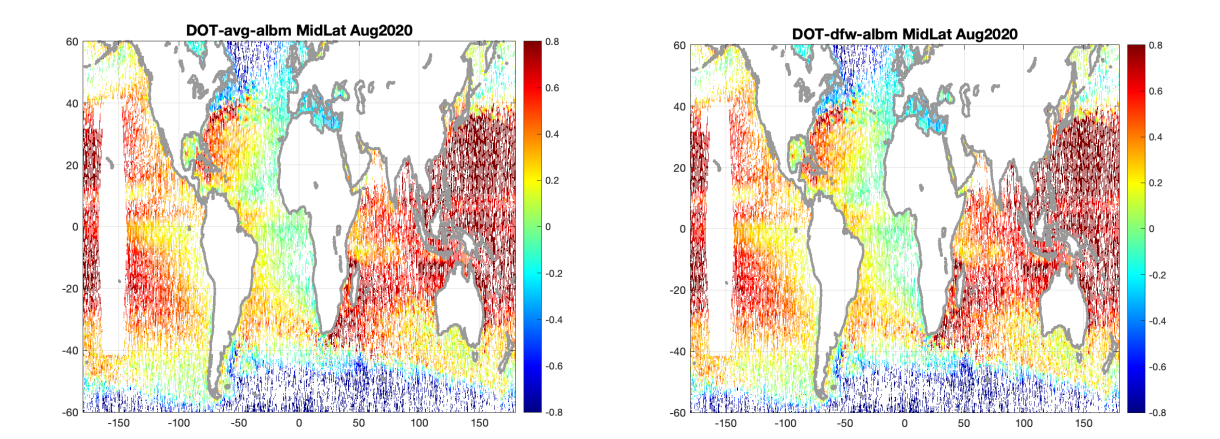


Figure 8. Mid-latitude DOT gridded by simple "n-segment" all-beam averages (left) and degree-of-freedom weighted (dfw) all-beam averages (right) for August 2020. The ocean scan region in the Central Pacific is not gridded.

All-beam quantities will mirror the single beam totals and averages of section 3.2.4.2 and use the same names with the suffix "\_albm" appended (See Table 3). The all-beam variables are computed in the same way the single beam variables are computed except all the ocean segments from all beams in a grid cell are used in the computation. These values should be the same as appropriately weighted averages of grid cell single beam averages (See Appendix D).

#### 3.2.4.4 Interpolation of DOT to Bin Centers

To compute the average DOT at the center of each grid cell, we perform least squares fit of a plane of the form dot = a\*x + b\*y + c to the ocean segment DOT in each cell plus the eight surrounding cells and evaluate the fitted plane at the center of the center cell. For a sensible solution we require data from at least two ICESat-2 orbits. It is due to the spacing of the orbits we look for data in nine cells; the center cell where we will compute the center-interpolated value and the eight cells surrounding that center cell. There must also be a minimum of four ocean segments in the 9 cells to compute a center-interpolated DOT value. Because we need as much data as possible to compute center values, all center values denoted by the suffix "cntr" will be derived using all beams. Further averages over the center cell and eight surrounding cells will be denoted by the suffix "9" and will be all-beam averages.

Note that in interpolating centered averages it is possible that center points can be on land, e.g., an island or peninsula. A land mask is provided as output to indicate if a center point for a centered average is in the ocean (*landmask*=0) or on land (*landmask*=1). While one would

not likely use the centered DOT value itself, the associated *a*, *b*, and *c* planar coefficients are from ocean data only, can be used to interpolate DOT in the water region surrounding the land, and are thus be of particular benefit to coastal oceanography and as a basis for optimal interpolation.

### 3.2.4.4.1 Average DOT at Bin Centers

*For the simple averages:* Computing averages interpolated to grid cell centers requires data from at least two orbits to get the required horizontal distribution of data to make a meaningful least-squares fit in space. The ICESat-2 orbital characteristics require that for a 1-month average at a grid cell center we must consider data in the surrounding 8 cells for a 9-cell fit.

For *n\_segs* greater than or equal to 4 from at least two orbits, assemble 1 by *n\_segs* vectors of the deviation of the DOT values from their average values, *dot\_avg9*, *lon\_avg9*, and *lat avg9*, where we are including the data from all nine cells for those averages.

$$h_i$$
'= (SSH- geoid\_seg-bin\_SSbias)-dot\_avg9  $i$ = 1 to  $n$  segs (45)

where *dot\_avg9* equals the 9-cell all-beam average of *(SSH-geoid\_seg-bin\_SSbias)* 

$$y_i$$
'= $lat_seg-lat_avg$ 9  $i=1 \text{ to } n_segs$  (47)

Referring to Appendix B, compute the cross product expected values  $L_{xx}$ ,  $L_{yy}$ ,  $L_{xy}$ ,  $R_{xh}$ , and  $R_{yh}$ :

$$L_{xx} = \sum_{i=1}^{N} x_{i}' x_{i}'$$

$$L_{yy} = \sum_{i=1}^{N} y_{i}' y_{i}' \quad \text{and} \quad R_{xh} = \sum_{i=1}^{N} x_{i}' h_{i}'$$

$$L_{xy} = \sum_{i=1}^{N} y_{i}' x_{i}'$$

$$R_{yh} = \sum_{i=1}^{N} y_{i}' h_{i}'$$

$$(48)$$

for *N* equal to *n\_segs*.

The coefficients defining the least-squares planar fit a, b, and c are given by

$$a = \frac{R_{xh}L_{yy} - R_{yh}L_{xy}}{L_{xx}L_{yy} - L_{xy}^{2}}$$

$$b = \frac{R_{yh}L_{xx} - R_{xh}L_{xy}}{L_{xx}L_{yy} - L_{xy}^{2}}$$

$$c = dot \quad ava9 - (a*lon \quad ava9 + b*lat \quad ava9)$$
(49)

The values of the planar fit coefficients, a, b, and c should be relabeled, saved, and output as a\_avg, b\_avg, and c\_avg because they can be used as the linear model of DOT in the grid cell. Together with the planar fits of all the other grid cells, they constitute a faceted linear model of DOT potentially over the whole world ocean that can form the basis model for optimal interpolation. The value of DOT at the center of the grid cell, **dot avgcntr** is then given by:

$$dot\_avgcntr = a\_avg * gridcntr\_lon + b\_avg * gridcntr\_lat + c\_avg$$
 (50)

To calculate the effective sea state bias, *ssb\_avgcntr*, we have to redo the calculation of the center value of DOT, *DOT\_avgnobias*, without the SSB correction using equation (45b) in place of (45):

$$h_i$$
'= (SSH- geoid\_seg)-dot\_avgnossb9,  $i$ = 1 to  $n$ \_segs (45b)

where *dot\_avgnossb9* equals the 9-cell all-beam average of (SSH- geoid\_seg)

Then the effective SSB at the cell center will be **ssb\_avgcntr** = DOT\_avgcntrnobias-**dot\_avgcntr**.

Calculate the uncertainty in the center average of DOT,  $\delta \hat{h} = dot\_avgcntr\_uncrtn$  in the planar fit estimate of DOT at the center position,  $\hat{x} = gridentr\_lon$ , and  $\hat{y} = gridentr\_lat$ , using equation (B14) of Appendix B for the uncertainty squared:

$$(\delta \hat{h})^{2} = (\delta \hat{h}_{0})^{2} \left( \left( \frac{1}{L_{a}} \right)^{2} \left( \left( L_{yy}^{2} L_{xx} - L_{yy} L_{xy}^{2} \right) (\hat{x}')^{2} + \left( L_{yy} L_{xx}^{2} - L_{xx} L_{xy}^{2} \right) (\hat{y}')^{2} \right) + 1 \right)$$
(B14)
$$\left( \frac{1}{L_{a}} \right)^{2} = \left( \frac{1}{L_{xx} L_{yy} - L_{xy}^{2}} \right)^{2}$$

Where  $\hat{x}' = \hat{x} - \overline{x}$  and  $\hat{y}' = \hat{y} - \overline{y}$  and the mean data location,  $\overline{x}$ ,  $\overline{y}$ , is **lon\_avg**, **lat\_avg**.

 $\delta \hat{h}_0$  is the uncertanty in height relative to the quality of the planar fit (QoF) computed from the sum of the squared error about the fit according to (B8) or in the absolute coordinate system:

$$QoF = \left( (N-2)^{-1} \sum_{i=1}^{N} \left( DOT_{seg} - \left( a_{avg} * lon_{seg} + b_{avg} * lat_{seg} + c_{avg} \right) \right)^{2} \right)^{\frac{1}{2}}$$

or

$$QoF = (n\_seg/(n\_seg-2))^{1/2} * RMS (DOT\_seg - (a\_avg*lon\_seg + b\_avg* lat\_seg+c\_avg)) (51)$$

To understand the effect of data spatial distribution on uncertainty, note that if the data point locations are randomly distributed, the x and y data positions are uncorrelated,  $L_{xy}$  is zero and (B14) becomes:

$$\delta \hat{h}^{2} = \delta \hat{h}_{0}^{2} \left( \frac{1}{L_{xx}L_{yy}} \right)^{2} \left( \left( L_{yy}^{2}L_{xx} \right) (\hat{x}')^{2} + \left( L_{yy}L_{xx}^{2} \right) (\hat{y}')^{2} + 1 \right)$$

$$= \delta \hat{h}_{0}^{2} \left( \frac{(\hat{x}')^{2}}{L_{xx}} + \frac{(\hat{y}')^{2}}{L_{yy}} + 1 \right)$$

and the uncertainty increases away from the average data position as the ratio of extrapolation distance,  $\hat{x}'$ , to the RMS spread of the data in x,  $L_{xx}^{1/2}$  and the ratio of extrapolation distance,  $\hat{y}'$ , to the RMS spread of the data in y,  $L_{yy}^{1/2}$ .

Conversely, if the x and y positions of the data are highly correlated, for example because

they are on a single straight line, the correlation coefficient,  $\begin{pmatrix} L_{xy}^2 \\ L_{xx}L_{yy} \end{pmatrix}^{1/2}$  approaches 1,  $L_a$ 

approaches zero, and the uncertainty becomes very large, especially for center positions well to the side of the correlated cloud of data points.

Therefore, we edit the centered average values with excessive uncertainty, dot\_avgcntr\_uncrtn > a value estimated from examination of distributions of dot\_avgcntr\_uncrtn to exceed more than 95% of dot\_avgcntr\_uncrtn values. We expect this value to be around 0.2 m.

**DOT\_seg** = ocean segment DOT data within the 9 cells and all beams

*lat\_seg*= latitudes of the ocean segments in the 9 cells and all beams for the mid-latitude grid. For the polar grids substitute the y-coordinate, *v seg*.

 $lon\_seg$  =longitudes of the ocean segments in the 9 cells and all beams for the mid latitude grid. For the polar grids substitute the x-coordinate, x seg.

### 3.2.4.4.2 Degree-of-Freedom-Uncertainty Weighted DOT at Bin Centers

For the degree of freedom weighted averages: Compute the average of degree-of-freedom-uncertainty weighted DOT at the center of each grid cell, assemble 1 by **n\_segs** vectors of the deviation of the DOT values from their degree-of-freedom-uncertainty weighted average values, **dot\_dfw9**, **lon dfw9**, and **lat dfw9**, again using all-beam data from 9 (3x3) cells.

$$h_i$$
"= (SSH- geoid\_seg-bin\_SSbias- dot dfw9),  $i$ = 1 to  $n$  segs (52)

where *Wi* equals (*h\_uncrtn*)-2 for the i<sup>th</sup> ocean segment (Note: In ice covered waters, *ice\_conc*> or equal to 15%, where we substitute *h\_ice\_free* for *h-geoid\_seg-bin\_ssbias*, we will also substitute the uncertainty in *h\_ice\_free*, *h\_ice\_free\_uncrtn*, for the uncertainty in *h*, *h\_uncrtn*. This will be critically important in the averaging schemes weighted by uncertainty for *dot\_dfw9* and companion *dfw9*-averaged variables). *dot\_dfw9* equals the 9-cell all-beam degree-of-freedom-uncertainty weighted average of *(SSH-geoid\_seg-bin\_SSbias)*. See *3.2.4.2.2*.

.

$$x_i$$
"= (lon\_seg - grid\_lon\_dfw9), i= 1 to n\_segs (53)

$$y_i$$
"= (lat\_seg - grid\_lat\_dfw9), i= 1 to n\_segs (54)

Referring to Appendix B, compute the cross product expected values  $L_{xxw}$ ,  $L_{yyw}$ ,  $L_{xyw}$ ,  $R_{xhw}$ , and  $R_{yhw}$  using equations (B17).

The coefficients defining the weighted least-squares planar fit  $(a_w, b_w, and c_w)$  are given by (B18). Relabel, save, and output the coefficients so that  $a_d f w = a_w$ ,  $b_d f w = b_w$ , and  $c_d f w = c_w$ . The degree-of-freedom-uncertainty weighted value of DOT interpolated to the center of the grid cell, *dot dfwentr* is then given by:

$$dot_dfwcntr = a_dfw * gridcntr_lon + b_dfw * gridcntr_lat + c_dfw$$
 (54)

To calculate the effective sea state bias, *ssb\_dfwcntr*, we must redo the calculation of the center value of DOT, *DOT\_dfwcntrnobias*, without the SSB correction using equation (52b) in place of (52):

$$h_i$$
"= (SSH- geoid\_seg - dot\_dfwnossb9),  $i$ = 1 to  $n$ \_segs (52b)

where **dot\_dfwnossb9** equals the 9-cell all-beam degree-of-freedom weighted average of **(SSH-geoid\_seg)**.

Then the effective SSB at the cell center will be **ssb\_dfwcntr** = DOT\_dfwcntrnobias-**dot\_dfwcntr**.

Calculate and output the uncertainty the weighted center average of DOT,  $\delta \hat{h}_w = dot\_dfwcntr\_uncrtn$  in the weighted planar fit estimate of DOT at the center position,  $\hat{x} = gridcntr\_lon$ , and  $\hat{y} = gridcntr\_lat$ , using equation (21) of Appendix B for the uncertainty squared:

$$\left(\delta \hat{h}_{w}\right)^{2} = \left(\delta \hat{h}_{0w}\right)^{2} \left\{ \left(\frac{1}{L_{aw}}\right)^{2} \left[ \left(L_{yyw}^{2} L_{xxw} - L_{yyw} L_{xyw}^{2}\right) (\hat{x}^{"})^{2} + \left(L_{xxw}^{2} L_{yyw} - L_{xxw} L_{xyw}^{2}\right) (\hat{y}^{"})^{2} \right] + 1 \right\}$$
 (B21)

where

$$\left(\frac{1}{L_{aw}}\right)^2 = \left(\frac{1}{L_{xxw}L_{yyw} - L_{xyw}^2}\right)^2$$

and  $\hat{x}'' = gridentr\_lon - grid\_lon\_dfw9$  and  $\hat{y}'' = gridentr\_lat - grid\_lat\_dfw9$  and  $\delta \hat{h}_{0w}$  is the uncertanty in height relative to the weighted planar fit computed from the sum of the weighted squared error about the weighted fit according to (B19), or in the absolute coordinate system:

$$(\delta \hat{h}_{0w})^{2} = (N/(N-2)) \left( \sum_{i=1}^{N} Wi \right)^{-1} \sum_{i=1}^{N} \left( Wi \left( DOT_{seg} - \left( a_{dfw} * lon_{seg} + b_{dfw} * lat_{seg} + c_{dfw} \right) \right)^{2} \right)$$
(55)

for

where,  $a_{dfw}$  denotes  $a_{-}dfw$ ,  $b_{dfw}$  denotes  $b_{-}dfw$ ,  $c_{dfw}$  denotes  $c_{-}dfw$ , and  $DOT_{seg}$  denotes  $DOT_{seg}$  = ocean segment DOT data within the 9 cells and all beams  $lat_{seg}$  denotes  $lat_{-}seg$  = latitudes of the ocean segments in the 9 cells and all beams  $lon_{seg}$  denotes  $lon_{-}seg$  = longitudes of the ocean segments in the 9 cells and all beams We will term  $\delta \hat{h}_{0w}$  the weighted quality of fit, QoFw

We edit the centered weighted average values with excessive uncertainty, *dot\_dfwcntr\_uncrtn* > a value estimated from examination of distributions of *dot\_dfwcntr\_uncrtn* to exceed more than 95% of *dot\_avgcntr\_uncrtn* values. We expect this value to be around 0.2 m.

### 3.2.4.4.3 One-month ATL19 and Three-month ATL23 Centered Averages

Figure 9 shows DOT grid averages interpolated to cell centers using Equations (45)-(50) for 1-month ATL19, August 2020, (Figure 9, left) and 3-months ATL23, Jul.-Aug.-Sept. 2020, (Figure 9, right). The results are similar for degree-of-freedom averaging Section 3.2.4.4.2, Equations (51)-(54). Even at 1-month, the spatial averaging of the 9-cell fit results in significantly fewer empty cells than the simple averages (Figure 8, left). Furthermore, the 91-day repeat of ICESat-2 including 1397 orbits, with two equator crossings per orbit each, results in an equator crossing every 0.13 degrees of longitude, so that every \( \frac{1}{4} \)° grid cell has the potential, barring clouds, to

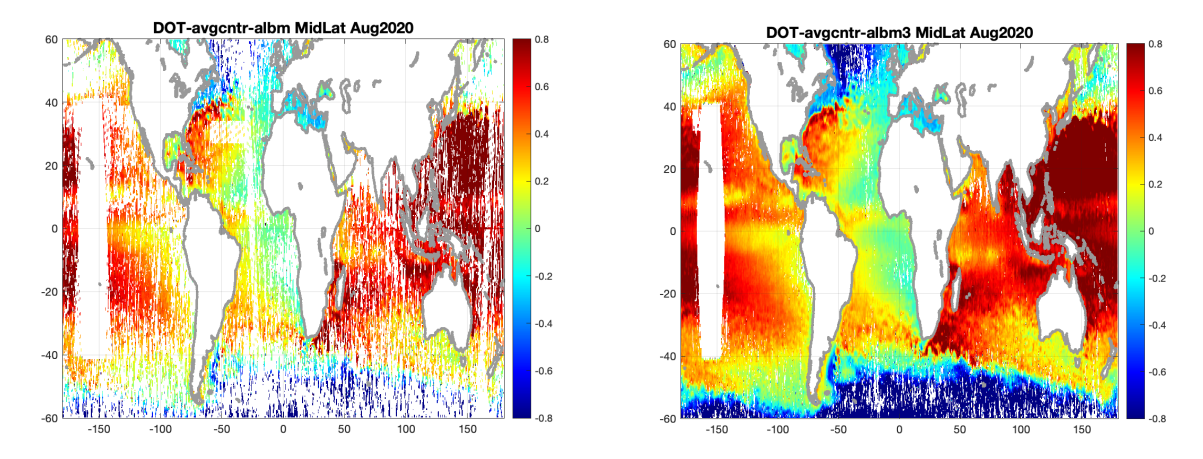


Figure 9. Centered grid averages using 9-cells (3x3) to fit to the center of a center cell for 1-month ATL19, August 2020, (left) and 3-month ATL23, Jul-Aug-Sept. 2020, (right).

see at least one satellite pass in 3 months, Consequently, almost every grid cell is filled in the 3-month centered average for July-Sept. 2020 (Figure 9, right). The 3-month centered average (Fig. 9, right) and degree-of-freedom weighted average will be good candidate background fields for optimal interpolation to finer spatial and temporal scales (Appendix E).

#### 3.2.5 Gridding Output

Output of the ATL19 gridding process will come in three latitude groups: mid-latitude, north-polar, and south-polar for the three grid systems (Section 3.2.1). A hierarchy of the ATL12 and ATL19 variables is given in Appendix D. The generic list of output variables applicable to each latitude group is given in Table 3. The grid sizes vary with region: mid-latitude [480 x 1440] (y-index, x-index), north-polar [448 x 304] and south-polar [332 x 316].

Table 3: ATL19 Outputs per Latitude Group

As indicated by "\_"\_albm, albm versions of the variables are also included

\* Indicates in single beam groups only

ATL19 Variable	Dimensions	Units	<u>Description</u>	Input ATL12
Name	mid-lat,	<u>Onits</u>	<u>Description</u>	Variable Name
<u>ivaiiic</u>	north-polar,			variable maine
	south-polar			
a ava	480 x 1440	m/deg	The a coefficient of the planar fit	
a_avg	448 x 304	m/m	used to compute dot avgentr	
	332 x 316	m/m	values	
	INVALID_R8B			
b_avg	480 x 1440	m/deg	The b coefficient of the planar fit	
	448 x 304	m/m	used to compute dot_avgcntr	
	332 x 316	m/m	values	
e ava	INVALID_R8B 480 x 1440	m	The c coefficient of the planar fit	
c_avg	448 x 304	m	used to compute dot avgentr	
	332 x 316	m	values	
	INVALID_R8B			
a_dfw	480 x 1440	m/deg	The a coefficient of the planar fit	h_uncrtn;
	448 x 304	m/m	used to compute dot_dfwcntr	or
	332 x 316	m/m	values	h_ice_free_uncrtn
b_dfw	INVALID R8B 480 x 1440	m/deg	The <i>b</i> coefficient of the planar fit	for IC>15%.  h uncrtn;
v_ujw	448 x 304	m/m	used to compute dot dfwcntr	n_uncrin, or
	332 x 316	m/m	values	h ice free uncrtn
	INVALID_R8B			for IC>15%.
c_dfw	480 x 1440	m	The c coefficient of the planar fit	h_uncrtn;
	448 x 304	m	used to compute dot_dfwcntr	or
	332 x 316 INVALID R8B	m	values	h ice free uncrtn for IC>15%.
	INVALID_Rob			101 1C> 1370.
delta time beg	1	seconds	Earliest time in grid	delta time
delta_time_end	1	seconds	Latest time in grid	delta_time
depth_avg	480 x 1440	meters	Simple average of ocean depth	depth_ocn_seg
"_"_albm	448 x 304			
	332 x 316			
depth dfw	INVALID_R4B 480 x 1440	meters	Degree-of-freedom-uncertainty	depth ocn seg
" " albm	448 x 304	meters	weighted average of ocean depth	uepin_ocn_seg
	332 x 316		weighted average of occan deput	
	INVALID R4B			
dof	480 x 1440	counts	Sum of degrees of freedom in	np_effect
dof_albm	448 x 304		surface height measurements,	
	332 x 316		which depends on along-track	
	INVALID_R8B		correlation length scale among 10-	
			m bin average heights	

dot_avg "_"_albm  dot_avginice_07_al bm	480 x 1440 448 x 304 332 x 316 INVALID_R8B 448 x 304 332 x 316 INVALID_R4B	meters	Simple average of dynamic ocean topography. For ice concentration >15%, <i>h_ice_free</i> is substituted <i>for h-geoidseg – bin ssbias</i> Simple average of ocean segment, <i>h_atl07_ice_free</i> DOT from ATL07 bright-lead segments in common with ATL12 10-m bins for IC> or = 15%	h-geoid_seg- bin_ssbias; h_ice_free for IC>15%. h atl07 ice free, ATL12 for IC>15%.
dot_avginice_07_u ncrtn_albm	448 x 304 332 x 316 INVALID_R4B	meters	Simple average of ocean segment, h_atl07_ice_free DOT uncertainties, h_atl07_ice_free_uncrtn from ATL07 bright-lead segments in common with ATL12 10-m bins for IC> or = 15%	h_atl07_ice_free_u ncrtn, ATL12 for IC>15%.
dot_avginice_7in1 2_albm	448 x 304 332 x 316 INVALID_R4B	meters	Simple average of ocean segment, h atl07 inatl12oc DOT in all bright-lead ATL07 sea ice segments in the ATL12 ocean segments for IC> or = 15%	h_atl07_inatl12oc, ATL12 for IC>15%.
dot_avginice_7in1 2_uncrtn_albm	448 x 304 332 x 316 INVALID_R4B	meters	Simple average of ocean segment, h_atl07_inatl12oc DOT uncertainties, h_atl07_inatl12oc_uncrtn, dependent variability in ATL07 bright-lead ATL07 sea ice segments defined for IC> or = 15%	h_atl07_inatl12oc_ uncrtn, ATL12 for IC>15%.
dot_icefree_avg_al bm	448 x 304 332 x 316 INVALID_R4B	meters	Simple average of ocean segment, $h\_ice\_free$ DOT in all bright-lead 10-m bins in the ATL12 ocean segments for IC> or = 15%	h_ice_free
dot_icefree_uncrtn _albm	448 x 304 332 x 316 INVALID_R4B	meters	Simple average of ocean segment, $h\_ice\_free\_uncrtn$ DOT uncertainties in all bright-lead 10-m bins in the ATL12 ocean segments for IC> or = 15%	h_ice_free_uncrtn
dot_avg_uncrtn "_"_albm	480 x 1440 448 x 304 332 x 316 INVALID_R4B R8B	meters	Average of ocean segment height uncertainties dependent on waves in open water and variability in and among bright-lead 10-m bins if IC>15% Uncertainty average of dynamic ocean topography	np_effect h var; h ice free uncrtn for IC>15%.
dot_avgcntr	480 x 1440 448 x 304 332 x 316 INVALID_R8B	meters	Simple all-beam average of dynamic ocean topography interpolated to center of grid cell. For ice concentration >15%, h_ice_free is substituted for h-geoidseg – bin_ssbias.	h-geoid_seg- bin_ssbias; h_ice_free for IC>15%.

dot_avgcntr_uncrt n	480 x 1440 448 x 304 332 x 316 INVALID_R8B	meters	Uncertainty of simple all-beam average of dynamic ocean topography interpolated to center of grid cell equal to the standard deviation of ocean segment DOT about planar fit.	h-geoid_seg- bin_ssbias; h ice free for IC>15%.
dot_dfw "_"_albm	480 x 1440 448 x 304 332 x 316 INVALID_R8B	meters	Degree-of-freedom-uncertainty Degree of freedom weighted by the uncertaintyaverage of the ocean segment dynamic ocean topography weighted by <i>h_unctn</i> for IC<15%, and <i>h_ice_free_uncrtn</i> for IC>15%.	h-geoid_seg, bin_ssbiasg h_ice_free for IC>15%.
dot_dfw_uncrtn "_"_albm	480 x 1440 448 x 304 332 x 316 INVALID_R8B	meters	Uncertainty of degree-of-freedom-uncertaintyDegree of freedom weighted average of dynamic ocean topography uncertaintyweighted by <i>h unctn</i> for IC<15%, and <i>h ice free uncrtn</i> for IC>15%.	h-geoid seg- bin_ssbias; h ice free for IC>15% and h uncrtn; or h_ice_free_uncrtn for IC>15%.
dot_dfwcntr	480 x 1440 448 x 304 332 x 316 INVALID_R8B	meters	Degree-of-freedom-uncertainty Degree of freedom weighted all=beam average dynamic ocean topography interpolated to center of grid cell weighted by <i>h_unctn</i> for IC<15%, and <i>h ice free uncrtn</i> for IC>15%.	h-geoid_seg- bin_ssbias; h_ice_free for IC>15%.
dot_dfwcntr_uncrt n	480 x 1440 448 x 304 332 x 316 INVALID_R8B	meters	Uncertainty in degree-of-freedom- uncertainty weighted all-beam average dynamic ocean topography interpolated to center of grid cell	h-geoid seg- bin_ssbias; h ice free for IC>15% and h uncrtn; or h_ice_free_uncrtn for IC>15%.
dot_hist "_"_albm	3001x480 x 1440 3001x448 x 304 3001x332 x 316 INVALID_R4B	counts	AllSingle beam aggregate probability density function of DOT from photon heights histograms (ATL12 <i>Y</i> histogram + <i>measnoffit2</i> ). Histogram bin centers are given by <i>ds_hist_bincenters</i> for each of the three grids.	y
dot_kurt_avg*	480 x 1440 448 x 304 332 x 316 INVALID R8B	none	Simple average of excess kurtosis of the dynamic ocean topography	h_kurtosis

dot_kurt_dfw*	480 x 1440 448 x 304 332 x 316 INVALID_R8B	none	Degree of freedom weighted average of excess kurtosis of the dynamic ocean topography (i.e., per description for dot_dfw, weighting by h_unctn for IC<15%, and h_ice_free_uncrtn for IC<15%)	h_kurtosis
dot_sigma_avg "_"_albm	480 x 1440 448 x 304 332 x 316 INVALID_R8B	meters	Simple average of the standard deviation of dynamic ocean topography	h_var
dot_sigma_dfw "_"_albm	480 x 1440 448 x 304 332 x 316 INVALID_R8B	meters	Degree-of-freedom-uncertainty Degree of freedom weighted average of the standard deviation of the dynamic ocean topography (i.e., per description for dot_dfw, weighting by h_unctn for IC<15%, and h_ice_free_uncrtn for IC>15%)	h_var
dot_skew_avg*	480 x 1440 448 x 304 332 x 316 INVALID R8B	none	Simple average of the skewness of dynamic ocean topography	h_skewness
dot_skew_dfw*	480 x 1440 448 x 304 332 x 316 INVALID R8B	none	Degree-of-freedom-uncertainty Degree of freedom weighted average of the skewness of dynamic ocean topography	h_skewness
ds_grid_x	304 (N) 316 (S)	meters	Center x value of polar grid cell	defined
ds_grid_y	448 (N) 332 (S)	meters	Center y value of polar grid cell	defined
ds_hist_bincenters	3001	meters	Bin centers for DOT aggregate histograms, <i>dot_hist</i> , from -15m to +15m in 1-cm bins.	ds_y_bincenters
geoid_avg "_"_albm	480 x 1440 448 x 304 332 x 316 INVALID_R8B	meters	Simple average of geoid height	geoid_seg
geoid_dfw "_"_albm	480 x 1440 448 x 304 332 x 316 INVALID_R8B	meters	Degree-of-freedom-uncertainty Degree of freedom weighted average of geoid height (i.e., per description for dot dfw, weighting by h_unctn for IC<15%, and h ice free uncrtn for IC>15%)	geoid_seg h_uncrtn; or h ice free uncrtn for IC>15%.
gridentr_lat	480 x 1440 448 x 304 332 x 316	°N	Latitude of grid cell center	defined
gridentr_lon	480 x 1440 448 x 304 332 x 316	°E	Longitude of grid cell center	defined

h_bias12rel07	448 x 304 x20 332 x 316 x 20	m	Distribution of $h\_ice\_free$ minus $h\_atl07\_inatl12oc$ versus ice concentration 5% to $\leq 10\%$ , $\geq 10\%$ to $\leq 15\%$ , $\geq 95\%$ to $\leq 100\%$	h_ice_free, h_atl07_inatl12oc
h_bias12rel07_nse gs	448 x 304 x20 332 x 316 x 20	none	Number of ocean segments that went into each $h\_bias12rel07$ ice concentration bin for each grid cell	h ice free, h_atl07_inatl12oc
h_bias12rel07_ttl	1x20 1x20	m	Aggregate over all grid cells in each Polar grid of $h\_bias12rel07$ versus ice concentration 5% to $\leq 10\%$ , $>10\%$ to $\leq 15\%$ , > 95% to $\leq 100\%$	h_ice_free, h_atl07_inatl12oc
h_bias12rel07_ttl_ nsegs.	1x20 1x20	none	Number of ocean segments that went into each <i>h</i> bias 12 rel07 ttl ice concentration bin for all grid cells for each Polar grid	h_ice_free, h_atl07_inatl12oc
h_icetop_geoid_av g_albm	448 x 304 332 x 316 INVALID_R4B	m	Height of the top of the ice taken from <i>h-geoid_seg-bin_ssbias</i> in ice-covered waters	h, geoid_seg
h_icetop_geoid_av g_uncrtn_albm	448 x 304 332 x 316 INVALID_R4B	m	Average uncertainty in height of the top of the ice taken from <i>h</i> -geoid_seg-bin_ssbias in ice-covered waters	H_uncrtn
latitude	480	°N	Vector of grid center latitude common values for all mid-latitude grid cells	defined
landmask	480 x 1440 448 x 304 332 x 316	none	A land mask to indicate if a center point for a 9-cell centered average is on land 1=ocean, 0=land), for example an island. While one would not use the centered DOT value, the <i>a, b,</i> and <i>c</i> coefficients are from ocean data only and can be used to interpolate DOT in the water region of the grid cell.	
latitude	480	°N	Vector of grid center latitude common values for all mid-latitude grid cells	defined
lat_avg "_"_albm	480 x 1440 448 x 304 332 x 316 INVALID R8B	°N	Simple average of latitude	latitude
lat_dfw "_"_albm	480 x 1440 448 x 304 332 x 316 INVALID_R8B	°N	Degree-of-freedom-uncertainty Degree of freedom weighted average of latitude (i.e., per description for <i>dot dfw</i> , weighting by <i>h_unctn</i> for IC<15%,	lLatitude h_uncrtn; or h ice free uncrtn for IC>15%.

			and <i>h_ice_free_uncrtn</i> for IC>15%)	
length_dfw "_"_albm	480 x 1440 448 x 304 332 x 316 INVALID_R4B	meters	DFW average of ocean segment length.	
length_sum "_"_albm	480 x 1440 448 x 304 332 x 316 INVALID_R48 B	meters	Sum of ocean segment lengths	length_seg
longitude	1440	°E	Vector of all center longitude common values for all mid-latitude grid cell	defined
lon_avg "_"_albm	480 x 1440 448 x 304 332 x 316 INVALID_R8B	°E	Simple average of longitude	longitude
lon_dfw "_ "_ albm	480 x 1440 448 x 304 332 x 316 INVALID_R8B	°E	Degree-of-freedom-uncertainty Degree of freedom weighted average of longitude (i.e., per description for <i>dot_dfw</i> , weighting by <i>h_unctn</i> for IC<15%, and <i>h_ice_free_uncrtn</i> for IC>15%)	longitude h uncrtn; or h_ice_free_uncrtn for IC>15%.
n_ph_srfc "_"_albm	480 x 1440 448 x 304 332 x 316 INVALID_I8B	counts	The sum of the number of surface reflected photons, <i>n_photons</i> , for all ocean segments in the grid cell.Sum of surface reflected photons	n_photons
n_phs_ttl "_"_albm	480 x 1440 448 x 304 332 x 316 INVALID_I8B	counts	The grid cell-total of all photons in the downlink bands, <i>n_ttl_photon</i> Sum of surface reflected photons plus rejected photons	n_ttl_photon
n_segs "_"_albm	480 x 1440 448 x 304 332 x 316 INVALID_I4B	counts	The nNumber of ocean segments in grid cell	
podppd_flag_prent "_"_albm	480 x 1440 448 x 304 332 x 316 INVALID_R4BI NVALID_I4B	percent	Percentage of ocean segments with nonzero (i.e., 4, nominal calibration maneuver) <i>podppd flag seg</i> used in the grid cell.	podppd_flag_seg
r_noise "_"_albm	480 x 1440 448 x 304 332 x 316 INVALID_R8B	count/met er	Simple average of photon noise rate	photon_noise_rate

r_srfc "_"_albm	480 x 1440 448 x 304 332 x 316 INVALID R8B	count/met er	Simple average of surface reflected photon rate	photon_rate
surf_prent_avg "_"_albm	5x[ 480 x 1440 448 x 304 332 x 316]	percent	The averages of the percentages of each <b>surface</b> type in the grid cell ocean segment as a 5-element variable with each element corresponding to the percentage of each of the 5 surface types.	surf_type_prcnt
ssb_avgcntr	480 x 1440 448 x 304 332 x 316 INVALID R8B	meters	Simple all-beam average of sea state bias interpolated to center of grid cell per the ATBD	bin_ssbias
ssb_dfw "_"_albm	480 x 1440 448 x 304 332 x 316 INVALID_R8B	meters	Degree-of-freedom-uncertainty Degree-of-freedom weighted average of sea state bias. (i.e., per description for <i>dot_dfw</i> , <i>h_unctn</i> for IC<15%, and <i>h_ice_free_uncrtn</i> for IC>15%)	bin_ssbias h_uncrtn; or h_ice_free_uncrtn for IC>15%.
ssb_dfwcntr	480 x 1440 448 x 304 332 x 316 INVALID_R8B	meters	Degree-of-freedom-uncertainty Degree-of-freedom weighted all- beam average of sea state bias interpolated to center of grid cell per the ATBD (i.e., per description for <i>dot dfw</i> , <i>h unctn</i> for IC<15%, and <i>h_ice_free_uncrtn</i> for IC>15%)	bin ssbias h uncrtn; or h_ice_free_uncrtn for IC>15%.
surf_prent_avg "_"_albm	5x[ 480 x 1440 448 x 304 332 x 316] INVALID_R4B	percent	The averages of the percentages of each <b>surface</b> type in the grid cell ocean segment as a 5-element variable with each element corresponding to the percentage of each of the 5 surface types.	surf_type_prcnt
surf_prent_dfw "_"_albm	5x[ 480 x 1440 448 x 304 332 x 316] INVALID_R4B	percent	The dfw averages of the percentages of each <b>surface</b> type in the grid cell ocean segment as a 5-element variable with each element corresponding to the percentage of each of the 5 surface types. (i.e., per description for <i>dot dfw</i> , weighting by <i>h unctn</i> for IC<15%, and <i>h_ice_free_uncrtn</i> for IC>15%)	surf_type_prcnt h uncrtn; or h_ice_free_uncrtn for IC>15%.
swh_avg "_"_albm	480 x 1440 448 x 304 332 x 316 INVALID R8B	meters	Simple average of the significant wave height	swh
swh_dfw	480 x 1440 448 x 304	meters	Degree-of-freedom-uncertainty Degree of freedom weighted	swh h_uncrtn;

"_"_albm	332 x 316 INVALID_R8B	average of the significant wave height (i.e., per description for dot dfw, h unctn for IC<15%, and h ice free uncrtn for IC>15%)	or h_ice_free_uncrtn for IC>15%.

### 3.3 Gridding DOT for ATL23

The ATL23 processing is identical to the ATL19 section 3.2 processing except there are a 3-month span of ATL12s input.

### References

Morison, J. H., D. Hancock, S. Dickinson, J. Robbins, L. Roberts, R. Kwok, S. Palm, B. Smith, M. Jasinski, and I.-S. Team. (2019), ATLAS/ICESat-2 L3A Ocean Surface Height, Version 2*Rep.*, NASA National Snow and Ice Data Center Distributed Active Archive Center, Boulder, Colorado USA..

Neumann, T. A., A. Brenner, D. Hancock, J. Robbins, J. Saba, K. Harbeck, A. Gibbons, J. Lee, S. B. Luthcke, T. Rebold, et al. (2021a). *ATLAS/ICESat-2 L2A Global Geolocated Photon Data, Version 4*. [Indicate subset used]. Boulder, Colorado USA. NASA National Snow and Ice Data Center Distributed Active Archive Center. doi: https://doi.org/10.5067/ATLAS/ATL03.004.

Luthcke, and T. Rebold (2021b), ICESat-2 Algorithm Theoretical Basis Document (ATBD) for Global Geolocated Photons ATL03, <a href="https://nsidc.org/sites/nsidc.org/files/technical-references/ICESat2">https://nsidc.org/sites/nsidc.org/files/technical-references/ICESat2</a> ATL03 ATBD r004.pdf

### **ACRONYMS**

ASAS ATLAS Science Algorithm Software

ATLAS Advance Topographic Laser Altimeter System

GSFC Goddard Space Flight Center

ICESat-2 MIS ICESat-2 Management Information System

IIP Instrument Impulse Response

MIZ Marginal Ice Zone PSO Project Science Office

PSO ICESat-2 Project Support Office

SDMS Scheduling and Data Management System
SIPS Science Investigator-led Processing System

TEP Transmit Echo Pulse

### **GLOSSARY**

### **APPENDIX A: ICESat-2 Data Products**

### ICESat-2 Data Products

File ID/Level	Product Name	Concept	Short Description	Frequency
00/0	Telemetry Data	Full rate Along- track with channel info	Raw ATLAS telemetry in Packets with any duplicates removed	Files for each APID for some defined time period
01/1A	Reformatted Telemetry	Full rate Along- track with channel info	Parsed, partially reformatted, time ordered telemetry. Proposed storage format is NCSA HDF5.	Uniform time TBD minutes (1 minute?)
02/1B	Science Unit Converted Telemetry	Full rate Along- track with channel info	Science unit converted time ordered telemetry. Reference Range/Heights determined by ATBD Algorithm using Predict Orbit and s/c pointing. All photon events per channel per pulse. Includes Atmosphere raw profiles.	Uniform time TBD minutes (1 minute?)
03/2A	Global Geolocated Photon Data	Full rate Along- track with channel info	Reference Range/Heights determined by ATBD Algorithm using POD and PPD. All photon events per pulse per beam. Includes POD and PPD vectors. Classification of each photon by several ATBD Algorithms.	Uniform time TBD minutes (1 minute?)
04/2A	Calibrated Backscatter Profiles	3 profiles at 25 Hz rate (based on 400 pulse mean)	Along-track backscatter data at full instrument resolution. The product will include full 532 nm (14 to -1.0 km) calibrated attenuated backscatter profiles at 25 times per second for vertical bins of approximately 30 meters. Also included will be calibration coefficient values for the polar region.	Per orbit
05/2B	Photon Height Histograms	Fixed distances Along-track for each beam	Histograms by prime Classification by several ATBD Algorithms. By beam	Uniform time TBD minutes (30 minutes?)
06/L3	Antarctica Ice Sheet Height / Greenland Ice Sheet Height	Heights calculated with the ice sheet algorithm, as adapted for a dH/dt calculation	Surface heights for each beam, along and across-track slopes calculated for beam pairs. All parameters are calculated for the same along-track increments for each beam and repeat.	There will be TBD files for each ice sheet per orbit

File ID/Level	Product Name	Concept	Short Description	Frequency
07/ L3	Arctic Sea Ice Height/ Antarctic Sea Ice Height	Along-track heights for each beam ~50- 100m (uniform sampling); separate Arctic and Antarctic products	Heights of sea ice and open water samples (at TBD length scale) relative to ellipsoid after adjusted for geoidal and tidal variations, and inverted barometer effects. Includes surface roughness from height statistics and apparent reflectance	There will be files for each pole per orbit
08/ L3	Land Water Vegetation Heights	Uniform sampling along-track for each beam pair and variable footpath	Heights of ground including inland water and canopy surface at TBD length scales. Where data permits, include estimates of canopy height, relative canopy cover, canopy height distributions (decile bins), surface roughness, surface slope and aspect, and apparent reflectance. (Inland water > 50 m length -TBD)	Per half (TBD) orbit
09/ L3	ATLAS Atmosphere Cloud Layer Characteristics	Based on 3 profiles at a 25 Hz rate. (400 laser pulses are summed for each of the 3 strong beams.)	Cloud and other significant atmosphere layer heights, blowing snow, integrated backscatter, optical depth	Per day
10/ L3	Arctic Sea Ice Freeboard / Antarctic Sea Ice Freeboard	Along-track all beams. Freeboard estimate along-track (per pass); separate Arctic/ Antarctic products	Estimates of freeboard using sea ice heights and available sea surface heights within a ~TBD km length scale; contains statistics of sea surface samples used in the estimates.	There will be files for each polar region per day
11/ L3	Antarctica Ice Sheet H(t) Series/ Greenland Ice Sheet H(t) Series	Height time series for pre-specified points (every 200m) along-track and Crossovers.	Height time series at points on the ice sheet, calculated based on repeat tracks and/or crossovers	There will be files for each ice sheet for each year
12/ L3A	Ocean Height	Along-track heights per beam for ocean including coastal areas	Height of the surface10 Hz/700 m (TBD) length scales. Where data permits, include estimates of height distributions (decile bins), surface roughness, surface slope, and apparent reflectance	Per half orbit
13/ L3	Inland Water Height	Along-track height per beam	Along-track inland ground and water height extracted from Land/Water/ Vegetation product. TBD data-derived surface indicator or mask. Includes roughness, slope and aspect.	TBD files Per day

File ID/Level	Product Name	Concept	Short Description	Frequency
14/L4	Antarctica Ice Sheet Gridded/ Greenland Ice Sheet Gridded	Height time series interpolated onto a regular grid for each ice sheet. Series (5- km posting interval)	Height maps of each ice sheet for each year of the mission, based on all available ICESat-2 data.	Per ice sheet per year
15/L4	Antarctica Ice Sheet dh/dt Gridded/ Greenland Ice Sheet dh/dt Gridded	Images of dH/dt for each ice sheet, gridded at 5 km.	Height-change maps of each ice sheet, with error maps, for each mission year and for the whole mission.	Per ice sheet for each year of mission, and for the mission as a whole
16/ L4	ATLAS Atmosphere Weekly	Computed statistics on weekly occurrences of polar cloud and blowing snow	Polar cloud fraction, blowing snow frequency, ground detection frequency	Per polar region Gridded 2 x 2 deg. weekly
17/ L4	ATLAS Atmosphere Monthly	Computed statistics on monthly occurrences of polar cloud and blowing snow	Global cloud fraction, blowing snow and ground detection frequency	Per polar region Gridded 1 x 1 deg. Monthly
18/L4	Land Height/ Canopy Height Gridded	Height model of the ground surface, estimated canopy heights and canopy cover gridded on an annual basis. Final high resolution DEM generated at end of mission	Gridded ground surface heights, canopy height and canopy cover estimates	Products released annually at a coarse resolution (e.g. 0.5 deg. tiles, TBD). End of mission high resolution (~1-2km)
19/ L4	Ocean MSS	Gridded monthly	Gridded ocean height product including coastal areas. TBD merge with Sea Ice SSH	Monthly

File	Product Name	Concept	<b>Short Description</b>	Frequency
ID/Level				

20/ L4	Arctic and Antarctic Gridded Sea Ice Freeboard/	Gridded monthly; separate Arctic and Antarctic products	Gridded sea ice freeboard. (TBD length scale)	Aggregate for entire month for each polar region
21/ L4	Arctic Gridded Sea Surface Height within Sea Ice/ Antarctic Gridded Sea Surface Height within Sea Ice	Aggregate for entire month (all sea surface heights within a grid) separate Arctic and Antarctic products	Gridded monthly sea surface height inside the sea ice cover. TBD grid	Aggregate for entire month for each polar region
22/L4	Inland water daily product			
23/ L4	Ocean MSS	Gridded monthly	Gridded ocean height product including coastal areas with 3-month moving average. TBD merge with Sea Ice SSH	Monthly
Experimental	Arctic Sea Ice Thickness / Antarctic Sea Ice Thickness	Per Pass Thickness samples (from 10- 100m freeboard means) for every 10 km (TBD) segment (all beams) where leads are available; (per pass)	Sea ice thickness estimates derived from the sea ice freeboard product. External input: snow depth and density for each pass.	There will be files for each polar region per day
Experimental	Arctic Gridded monthly Sea Ice Thickness / Antarctic Gridded monthly Sea Ice Thickness	Aggregate for entire month (all thickness observations within a grid) plus Thickness (corrected for growth)	Gridded sea ice thickness product; centered at mid-month. Include thickness with or without adjustment for ice growth (based on time differences between freeboard observation).	Gridded monthly (all thickness observations within a grid) for each polar region

Experimental	Lake Height	Along reference track per beam in Pan-Arctic basin (>50-60 deg N).	Extracted from Product 08 and 13, for lakes >10 km2, with slope and aspect. Ice on/off flag. TBD water mask developed from existing masks.	Monthly along track product, no pointing
Experimental	Snow Depth	Along reference track per beam for Pan-Arctic basin (>50-60 deg N).	Extracted from Product 08 and 13 along track repeat heights, with slope and aspect. Snow detection flag.	Monthly along track product, no pointing

### **APPENDIX B: Fitting a Plane to Spatially Distributed Data**

### **B.1** Average DOT

To evaluate the average DOT at the center of a grid cell we fit a plane to all the samples within the cell and the eight grid cells surrounding it and evaluate the height of the plane at the center of the center grid cell. To do this we first have to make a least-squares fit of a plane to DOT at N locations within the nine grid cells. Following *Eberly* (2019), given data (DOT) as a function of x and y,  $h_i = f(x_i, y_i)$  at i=1 to N locations, find a least squares fit of a plane, coefficients a, b, and c,

to 
$$h_i$$
 with mean,  $\overline{h} = \left(\frac{1}{N}\right) \sum_{i=1}^{N} h_i$ . (Also note  $\overline{x} = \left(\frac{1}{N}\right) \sum_{i=1}^{N} x_i$  and  $\overline{y} = \left(\frac{1}{N}\right) \sum_{i=1}^{N} y_i$ )

$$h_i \approx ax_i + by_i + c \tag{B1}$$

And we want to choose a, b, and c such that the error, E,

$$E(a,b,c) = \sum_{i=1}^{N} ((ax_i + by_i + c) - h_i)^2$$

is minimized. According to *Eberle* (2019) the solution is more robust, and the equations are simpler if we initially eliminate the need to determine c by taking the average of (B1) and subtracting it from (B1), to get:

$$h_i - \overline{h} \approx a(x_i - \overline{x}) + b(y_i - \overline{y})$$

and so for the deviations 
$$h'_i = h_i - \overline{h}$$
,  $x'_i = x_i - \overline{x}$ , and  $y'_i = y_i - \overline{y}$  (B2)

$$h_i' \approx ax_i' + by_i' \tag{B3}$$

and we will choose a and b to minimize:

$$E(a,b) = \sum_{i=1}^{N} ((ax_i' + by_i') - h_i')^2$$
 (B4)

Then c will be given by  $c = \overline{h} - (a\overline{x} + b\overline{y})$ . To minimize E with respect to a and b we find a and b for which:

$$\frac{\partial E(a,b)}{\partial a} = 2\sum_{i=1}^{N} x_i'((ax_i' + by_i') - h_i') = 2\sum_{i=1}^{N} ax_i'x_i' + bx_i'y_i' - x_i'h_i' = 0$$

$$\frac{\partial E(a,b)}{\partial b} = 2\sum_{i=1}^{N} y_i'((ax_i' + by_i') - h_i') = 2\sum_{i=1}^{N} ay_i'x_i' + by_i'y_i' - y_i'h_i' = 0$$

or

$$a\sum_{i=1}^{N} x_{i}'x_{i}' + b\sum_{i=1}^{N} x_{i}'y_{i}' = \sum_{i=1}^{N} x_{i}'h_{i}'$$

$$a\sum_{i=1}^{N} y_{i}'x_{i}' + b\sum_{i=1}^{N} y_{i}'y_{i}' = \sum_{i=1}^{N} y_{i}'h_{i}'$$

Letting

$$L_{xx} = \sum_{i=1}^{N} x_{i}' x_{i}'$$

$$L_{yy} = \sum_{i=1}^{n} y_{i}' y_{i}' \quad \text{and}$$

$$R_{xh} = \sum_{i=1}^{N} x_{i}' h_{i}'$$

$$L_{xy} = \sum_{i=1}^{N} y_{i}' x_{i}'$$

$$R_{yh} = \sum_{i=1}^{N} y_{i}' h_{i}'$$
(B5)

a, b, and c are given by

$$a = \frac{R_{xh}L_{yy} - R_{yh}L_{xy}}{L_{xx}L_{yy} - L_{xy}^{2}}$$

$$b = \frac{R_{yh}L_{xx} - R_{xh}L_{xy}}{L_{xx}L_{yy} - L_{xy}^{2}}$$

$$c = \overline{h} - (a\overline{x} + b\overline{y})$$
(B6)

### **Uncertainty in the Fit**

The uncertainty,  $\delta \hat{h}$ , in the planar fit estimate of height  $\hat{h}$  at  $x = \hat{x}$  and  $y = \hat{y}$ , is the uncertainty in

$$\hat{h}(\hat{x}, \hat{y}) = a(\hat{x} - \overline{x}) + b(\hat{y} - \overline{y}) + \hat{h}(\overline{x}, \overline{y})$$

$$\hat{h} = a\hat{x}' + b\hat{y}' + \hat{h}_0$$

where  $\hat{h}_0$  is the fit at the mean data position  $\overline{x}$ ,  $\overline{y}$ ,  $\hat{x}' = \hat{x} - \overline{x}$ , and  $\hat{y}' = \hat{y} - \overline{y}$ 

$$(\delta \hat{h})^2 = (\delta a \ \hat{x}')^2 + (\delta b \ \hat{y}')^2 + (\delta \hat{h}_0)^2$$
(B7)

This is related to the RMS residual squared.

$$(\delta \hat{h}(\overline{x}, \overline{y}))^{2} = (\delta \hat{h}_{0})^{2} = (N-2)^{-1} E(a,b) = (N-2)^{-1} \sum_{i=1}^{N} ((a \ x_{i}' + b \ y_{i}') - h_{i}')^{2}$$
(B8)

and the squared uncertainties in the slopes, a, and b related to the sensitivities of the slopes to the individual  $h_i$ , and the squared uncertainty in the  $h_i$ . Using the first of equations (B6)

$$(\delta a)^{2} = \sum_{i=1}^{N} \left( \frac{\partial a}{\partial h_{i}'} \delta h_{i}' \right)^{2} = \sum_{i=1}^{N} \left( \frac{\partial}{\partial h_{i}} \left( \frac{R_{xh} L_{yy} - R_{yh} L_{xy}}{L_{xx} L_{yy} - L_{xy}^{2}} \right) \delta h_{i}' \right)^{2}$$

$$(\delta a)^{2} = \left( \frac{1}{L_{a}} \right)^{2} \sum_{i=1}^{N} \left( \left( \frac{\partial R_{xh}}{\partial h_{i}} L_{yy} - \frac{\partial R_{yh}}{\partial h_{i}} L_{xy} \right) \delta h_{i}' \right)^{2}$$
(B9)

where

$$\left(\frac{1}{L_a}\right)^2 = \left(\frac{1}{L_{xx}L_{yy} - L_{xy}^2}\right)^2$$
 (B10)

and from (B5)

$$\frac{\partial R_{xh}}{\partial h_i} = \frac{\partial}{\partial h_i} \sum_{i=1}^{N} x_i' h_i' = x_i'$$

$$\frac{\partial R_{yh}}{\partial h_i} = \frac{\partial}{\partial h_i} \sum_{i=1}^{N} y_i' h_i' = y_i'$$
(B11)

plugging into (B9)

$$(\delta a)^2 = \left(\frac{1}{L_a}\right)^2 \sum_{i=1}^N \left(\left(x_i' L_{yy} - y_i' L_{xy}\right) \delta h_i'\right)^2$$

At this point we need to make an assumption about  $\delta h_i$ . We compute an uncertainty for each ocean segment,  $h\_uncrtn$ , based on the estimated degrees of freedom and height variance over the ocean segment. But this is only the uncertainty at the time and location of the measurement due to the wave induced, spatially correlated variations in height over the segment at the time of the segment. It doesn't include the uncertainty due to temporal and spatial variability of DOT.

The net uncertainty is probably better and more conservatively estimated as the residual error about the planar fit,  $(\delta \hat{h}_0)^2$ . Then

$$(\delta a)^2 = (\delta \hat{h}_0)^2 \left(\frac{1}{L_a}\right)^2 \sum_{i=1}^N \left(x_i' L_{yy} - y_i' L_{xy}\right)^2$$
 (B12)

Similarly

$$(\delta b)^{2} = (\delta \hat{h}_{0})^{2} \left(\frac{1}{L_{a}}\right)^{2} \sum_{i=1}^{N} \left(y_{i}^{\prime} L_{xx} - x_{i}^{\prime} L_{xy}\right)^{2}$$
(B13)

From (B7):

$$(\delta \hat{h})^{2} = (\delta a)^{2} (\hat{x}')^{2} + (\delta b)^{2} (\hat{y}')^{2} + (\delta \hat{h}_{0})^{2}$$

$$(\delta \hat{h})^{2} = (\delta \hat{h}_{0})^{2} \left(\frac{1}{L_{a}}\right)^{2} \sum_{i=1}^{N} (x_{i}' L_{yy} - y_{i}' L_{xy})^{2} (\hat{x}')^{2} + (\delta \hat{h}_{0})^{2} \left(\frac{1}{L_{a}}\right)^{2} \sum_{i=1}^{N} (y_{i}' L_{xx} - x_{i}' L_{xy})^{2} (\hat{y}')^{2} + (\delta \hat{h}_{0})^{2}$$

$$(\delta \hat{h})^{2} = (\delta \hat{h}_{0})^{2} \left(\frac{1}{L_{a}}\right)^{2} \left(\sum_{i=1}^{N} (x_{i}' L_{yy} - y_{i}' L_{xy})^{2} (\hat{x}')^{2} + (y_{i}' L_{xx} - x_{i}' L_{xy})^{2} (\hat{y}')^{2}\right) + 1$$

Expanding the sums:

$$(\delta \hat{h})^{2} = (\delta \hat{h}_{0})^{2} \left( \left( \frac{1}{L_{a}} \right)^{2} \left( \left( L_{yy}^{2} L_{xx} - L_{yy} L_{xy}^{2} \right) (\hat{x}')^{2} + \left( L_{yy} L_{xx}^{2} - L_{xx} L_{xy}^{2} \right) (\hat{y}')^{2} \right) + 1 \right)$$
(B14)

The square root of (B14) is the ATL19 variable *dot\_avgcntr\_uncrtn*.

It is useful to consider the uncertainty for particular distributions of data points. If the data point locations are randomly distributed, the *x* position and *y* position are uncorrelated, Lxy is zero and (B14) becomes:

$$\delta \hat{h}^{2} = (\delta \hat{h}_{0})^{2} \left( \frac{1}{L_{xx}L_{yy}} \right)^{2} \left( \left( L_{yy}^{2}L_{xx} \right) (\hat{x}')^{2} + \left( L_{yy}L_{xx}^{2} \right) (\hat{y}')^{2} + 1 \right)$$

$$= (\delta \hat{h}_{0})^{2} \left( \frac{(\hat{x}')^{2}}{L_{xx}} + \frac{(\hat{y}')^{2}}{L_{yy}} + 1 \right)$$

and the uncertainty increases away from the average data position as the ratio of  $\hat{X}'$  to the RMS spread of the data in x,  $L_{xx}^{1/2}$  and the ratio of  $\hat{y}'$  to the RMS spread of the data in y,  $L_{yy}^{1/2}$ . If the x and y positions of the data are highly correlated, for example because they are on a single

straight line, the correlation coefficient, 
$$\begin{pmatrix} L_{xy}^2 \\ L_{xx}L_{yy} \end{pmatrix}^{1/2}$$
 approaches 1,  $L_a$  approaches zero, and

the uncertainty becomes very large, especially for center positions well to the side of the correlated cloud of data points.

### **B.2** Degree-of-Freedom-Uncertainty Weighted Average DOT JWR - 20220621

This basically follows the algorithm already laid out in Appendix B.1 for the unweighted case.

The weights are provided by the ocean segment  $h\_uncrtn$  values. The weights are established as the inverse square of  $h\_uncrtn$  for each i<sup>th</sup> ocean segment going into the average:

$$w_i = \left[\frac{1}{(h_{uncrtn})^2}\right]_i$$

What this equation does is give stronger weight to lower values of **h\_uncrtn**. If an ocean segment's **h\_uncrtn** is 0.01 m, then it's weight will be 10000; if it is 0.1 m, it has a weight of 100, etc. A standard statistical practice is to adopt a one over the sigma squared as the weight [Citation Needed].

The weights are applied from the very beginning, with the computation of weighted mean locations and heights. Analogously to the equations found just before eq. B1, we have weighted mean values:

$$\bar{x}_{w} = \frac{\sum_{i=1}^{N} w_{i} x_{i}}{\sum_{i=1}^{N} w_{i}}$$

$$\bar{y}_{w} = \frac{\sum_{i=1}^{N} w_{i} y_{i}}{\sum_{i=1}^{N} w_{i}}$$
(B15)
$$\bar{h}_{w} = \frac{\sum_{i=1}^{N} w_{i} h_{i}}{\sum_{i=1}^{N} w_{i}}$$

Equation B2 is very similar, except now the weighted mean values are used. A double prime has been assigned to denote the weighted de-meaned values:

$$h''_{i} = h_{i} - \bar{h}_{w}, \ x''_{i} = x_{i} - \bar{x}_{w} \ and \ y''_{i} = y_{i} - \bar{y}_{w}$$
 (B16)

Similar to (B5), the equations (B17) for the weighted L's and R's are very similar to the unweighted case, now with an additional weighting multiplier,

$$L_{xxw} = \sum_{i=1}^{N} w_i \ x''_i \ x''_i$$

$$L_{yyw} = \sum_{i=1}^{N} w_i \ y''_i \ y''_i$$

$$L_{xyw} = \sum_{i=1}^{N} w_i \ x''_i \ y''_i$$

$$R_{xhw} = \sum_{i=1}^{N} w_i \ x''_i h''_i$$

$$R_{yhw} = \sum_{i=1}^{N} w_i \ y''_i h''_i$$
(B17)

The equations that give the coefficients for the planar fit are essentially the same in form as the weighted case except we replace the L & R terms with the weighted versions. Using a w-subscript for the coefficients computed when weights are applied, i.e.,  $a_w$ ,  $b_w$ ,  $c_w$ .

$$a_{w} = \frac{R_{xhw}L_{yyw} - R_{yhw}L_{xyw}}{L_{xxw}L_{yyw} - L_{xyw}^{2}}$$

$$b_{w} = \frac{R_{yhw}L_{xxw} - R_{xhw}L_{xyw}}{L_{xxw}L_{yyw} - L_{xyw}^{2}}$$

$$c_{w} = \bar{h}_{w} - (a_{w}\bar{x}_{w} + b_{w}\bar{y}_{w})$$
(B18)

The weighted version of equation (B8) is,

$$\left(\delta \hat{h}_{0w}\right)^{2} = (N/(N-2))(\sum_{i=1}^{N} w_{i})^{-1} \sum_{i=1}^{N} w_{i} [(a_{w} x_{i}^{*} + b_{w} y_{i}^{*}) - h_{i}^{*}]^{2}$$
(B19)

And for

$$\left(\frac{1}{L_{aw}}\right)^2 = \left(\frac{1}{L_{xxw}L_{yyw} - L_{xyw}^2}\right)^2 \tag{B20}$$

the uncertainty,  $(\delta \hat{h}_w)$  for the weighted centered average is:

$$\left(\delta \hat{h}_{w}\right)^{2} = \left(\delta \hat{h}_{0w}\right)^{2} \left\{ \left(\frac{1}{L_{aw}}\right)^{2} \left[ \left(L_{yyw}^{2} L_{xxw} - L_{yyw} L_{xyw}^{2}\right) (\hat{x}'')^{2} + \left(L_{xxw}^{2} L_{yyw} - L_{xxw} L_{xyw}^{2}\right) (\hat{y}'')^{2} \right] + 1 \right\}$$
(B21)

Where the cell center location is denoted by:  $\hat{x}'' = x_{cell \ center} - \bar{x}_w$  and  $\hat{y}'' = y_{cell \ center} - \bar{y}_w$ .

Eberle, D., 2019, Least Squares Fitting of Data by Linear or Quadratic Structures David Eberly, Geometric Tools, Redmond WA 98052

https://www.geometrictools.com/

This work is licensed under the Creative Commons Attribution 4.0 International License. To view a copy

of this license, visit <a href="https://creativecommons.org/licenses/by/4.0/">https://creativecommons.org/licenses/by/4.0/</a> or send a letter to Creative Commons,

PO Box 1866, Mountain View, CA 94042, USA.

Created: July 15, 1999

Last Modified: February 14, 2019

https://www.geometrictools.com/Documentation/LeastSquaresFitting.pdf

### **APPENDIX C: Hierarchy of ATL12 and ATL19/23 Variables**

#### ATL12 Inputs to ATL19/23

Segment Averages: SSH-geoid\_seg-bin\_ssbias, lat\_seg, lon\_seg, bin\_ssbias, geoid\_seg,

depth\_ocn\_seg, length\_seg, and surf\_type\_prcnt.
Segment Moments: SSHvar, SSHskew, SSHkurt, swh

Segment Histogram: Y, n photons

Segment Degrees-of-Freedom: NP effect

#### 3.2.4.2.1 Output ATL19/23 Averaging Over *n* segs Bins

Grid Cell Averages: dot avg, lat avg, lon avg, ssb avg, geoid avg, depth avg, surf prent avg

Grid Cell Average Moments: dot\_sigma\_avg, dot\_skew\_avg, dot\_kurt\_avg, swh\_avg

Grid Cell Total Histogram: dot hist

Grid Cell Totals: n\_segs, n\_phs\_ttl, n\_ph\_srfc ,length\_sum

Grid cell DOT Uncertainty: dot\_avg\_uncrtn

#### 3.2.4.2.2 Output ATL19/23 Averaging Weighted by Degrees-of-Freedom

Grid Cell Degree-of-Freedom Weighted Averages dot\_dfw, lat\_dfw, lon\_dfw, ssb\_dfw, geoid dfw, depth dfw, length dfw, surf prent dfw

Grid Cell Degree-of-Freedom Weighted Moments dot\_sigma\_dfw, dot\_skew\_dfw, dot kurt dfw, swh dfw

Grid Cell Degrees-of-Freedom and DOT Uncertainty: dof, dot dfw uncrtn

#### 3.2.4.3 Output ATL19/23 Merging All-Beam, variables

All single beam gridded variables have all-beam versions, except for gridded skewness and gridded kurtosis. The all-beam variable names end in 'albm'.

#### 3.2.4.4.1 Output ATL19/23 Interpolated to Bin Centers (gridentr lon and gridentr lat)

Averages at Grid Cell Center: dot avgcntr, ssb avgcntr

#### 3.2.4.4.2 Output ATL19/23 Interpolated to Bin Centers (gridentr and gridentr lat)

DOF Weighted Averages at Grid Cell Center: dot dfwcntr, ssb dfwcntr

### **APPENDIX D: All-beam Average Equivalencies**

The all-beam parameters can be computed in the same way single beam averages are computed by merely incorporating all the ocean segments from all beams in a grid cell. However the results should be the same as the properly weighted single beam averages as described below

.The photon all-beam (\*\_albm) totals are computed first. For all-beam total surface reflected photons, n\_ph\_srfcalbm add the number of surface reflected photons, n\_ph\_srfc, for each beam, and for the all-beam total of all photons in the downlink bands, n\_phs\_ttl\_albm, add the grid cell totals, n\_phs\_ttl, for each beam. Further, the all-beam photon rate, r\_srfc\_albm, is equal to n\_ph\_sfcalbm divided by length\_sum\_albm, the total of the total length of segments, length\_sum, for each beam. Similarly, the all-beam noise rate, r\_noise\_albm equals (n\_phs\_ttlalbm minus n\_ph\_srfcalbm) divided by length\_sum\_albm.

### **All-beam Average DOT**

The average DOT of data from all six beams in the cell, dot avg albm should equal.

The following variables have all-beam gridded simple averages that can be calculated in the same way: depth, geoid, lat, lon, ssb, surf\_prent and swh. The variable names all end in \_avg\_albm.

#### All-beam Degree-of-Freedom Weighted Average DOT

The degree-of-freedom average DOT of all six beams in the cell, *dot\_dfw\_albm* should equal

dot\_dfwalbm=

(Sum [dof\* dot dfwcntr]beams 1 to 6) / Sum [dof]beams 1 to 6,

For each grid cell we also can compute the all-beam degrees of freedom *dof\_albm*, the all-beam degree-of-freedom weighted standard deviation, *dot\_sigma\_dfwalbm*, and DOT uncertainty, *dot\_dfw\_uncrtn\_albm*.

 $dof\_albm = Sum [dof]_{beams 1 to 6}$ 

 $dot\_sigma\_dfwalbm = ((Sum [dof*(dot\_sigma\_dfw)^2]_{beams1 to 6}) / dof\_albm)^{1/2}$   $dot dfw albm uncrtn = dot sigma dfwalbm / (dof albm)^{1/2}$ 

# APPENDIX E: Optimal Interpolation of ICESat-2 Dynamic Ocean Topography

This section in anticipation of future ATL19/23 features is largely excerpted from Harry Stern's optimal interpolation notes, "HSnote1998", 7/2/1998 with additions from David Morison's Kriging series: "Kriging7\_JM", 2/23/2021.

#### **Optimal Interpolation**

We want to estimate or interpolate a true field of surface height or dynamic ocean topography, H(x), by an approximation  $\hat{H}$  of the form

$$\hat{H} = \sum_{i=1}^{n} a_i(x) \hat{H}_i \tag{E1}$$

In this expression:

x is a spatial coordinate. We could just as well have written H(x,y,z) to estimate H in 3-D. The number of spatial dimensions makes no difference in the following development. The coordinate x or coordinates x, y, z are just parameters.

 $\hat{H}_i$  are observations at spatial coordinate  $x_i$ .

 $a_j(x)$  are unknown functions that we will determine. We could just as well have written  $a_i(x,y,z)$  for the 3-D case.

So the estimate  $\hat{H}(x)$  is a linear combination of the measurements  $\hat{H}_j$ . We will sometimes drop the reference to the spatial coordinate x and just write H,  $\hat{H}$ , and  $a_j$  with the understanding that these depend on the spatial coordinates.

We suppose that each measurement,  $\hat{H}_j$ , consists of a true value  $H_j$  plus a measurement error  $\delta_j$ :

$$\hat{H}_j = H_j + \delta_j \tag{E2}$$

So  $H_j = H(x_j)$  is the true value of the field H(x) at the measurement point  $x_j$ .

Now we form the error expression between the true field and the estimate,  $\mathcal{E} = H - \hat{H}$ , using (E1) and (E2). We write  $\mathcal{E}^2$  as

$$\varepsilon^{2} = \left[ H - \sum_{j=1}^{n} a_{j} \left( H_{j} + \delta_{j} \right) \right]^{2}$$
 (E3)

At this point we introduce the idea of random variables. We consider the true value of H(x) to be an ensemble or collection of values, a random variable with some mean and variance. Similarly, the  $\mathcal{H}_j$  are random variables. The measurement errors,  $\delta_j$  are random variables with zero mean. The coefficients  $a_j$  are not random variables. We use the notation E[...] for the expected value of a random variable. We want to determine coefficients,  $a_j$ , by minimizing  $E\left[\varepsilon^2\right]$ . To minimize the error with respect to the  $a_j$ , we set the derivative of the error with respect to each coefficient equal to zero. Assuming the errors and true heights are uncorrelated, we find the n coefficients are given by a system of n equations for the n coefficients.

$$\sum_{j=1}^{n} \frac{E[H_{j}H_{k}]}{E[H^{2}]} a_{j} + \sum_{j=1}^{n} \frac{E[\delta_{j}\delta_{k}]}{E[H^{2}]} a_{j} = \frac{E[HH_{k}]}{E[H^{2}]}$$
(E4)

The expression  $E\left[\delta_j\delta_k\right]$  is the covariance of the measurement errors. If we make the assumption that the errors are uncorrelated then this term is zero when  $j\neq k$ , and we write  $E\left[\delta_k^2\right] = \sigma_k^2$  for the variance of the  $k^{th}$  measurement error. Then the second term in (E4) reduces to  $\frac{\sigma_k^2}{E[H^2]}a_k$ .

Now we return to the idea of the background or mean field. The expressions

$$\frac{E[H_j H_k]}{E[H^2]} \text{ and } \frac{E[H H_k]}{E[H^2]}$$
 (E5)

would be correlations if the mean of H were zero. Since we want to interpret them as correlations, we must insist that H have zero mean. Also  $E[H^2]$  is not a variance unless H has a zero mean. So we have to modify our thinking about H(x). We are free to construct any background field, B(x), that we like. And we may subtract B from H and  $\hat{H}$  to get the deviations from the background:

$$h=H-B$$
 and  $\hat{h}=\sum_{j=1}^{n}a_{j}\hat{h}_{j}$  where  $\hat{h}_{j}=\hat{H}_{j}-B(x_{j})$ 

We go through the derivation of (E4) with h and  $\hat{h}$  instead of H and  $\hat{H}$  and end up with terms corresponding to (E5):

$$\frac{E[h_j h_k]}{E[h^2]} \text{ and } \frac{E[h h_k]}{E[h^2]}$$
 (E6),

which are correlations because h has zero mean. So whatever background field we construct, it must be a mean field in the sense that it leaves zero mean fluctuations when subtracted from H(x) (in which case E[h] equals zero and  $E[\varepsilon^2]$  equals the variance of  $\varepsilon$ ).

We now return to (E4) and consider h (and  $h_j$ ) to be fluctuations from the background field B(x) such that E[h] equals zero. Note that this requires subtracting  $B_j$  (equal to  $B(x_j)$ ) from the measurements  $\hat{H}_j$ :

$$\hat{h} = \sum_{j=1}^{n} a_j \left( \hat{H}_j - B_j \right) \tag{E7}$$

and re-interpreting  $\hat{H}$  as well, i.e., adding  $B(x_j)$  to  $\hat{h}$  to obtain  $\hat{H}$ . With the assumption of uncorrelated measurement errors equation (E4) becomes:

$$\sum_{j=1}^{n} \frac{E\left[h_{j}h_{k}\right]}{E\left[h^{2}\right]} a_{j} + \frac{\sigma_{k}^{2}}{E\left[h^{2}\right]} a_{k} = \frac{E\left[hh_{k}\right]}{E\left[h^{2}\right]}$$
(E8)

or

$$(\mathbf{R} + \mathbf{D})\vec{a} = \vec{s} \tag{E9}$$

where we use the matrix notation to denote:

R = the correlation matrix of the fluctuation field between all pairs of locations where measurements are made. The (j,k) entry of this n x n symmetric matrix is  $E[h_j h_k]$  over  $E[h^2]$ .

**D** = the diagonal matrix with entries  $\sigma_k^2/E[h^2]$  giving the ratio of measurement error variance to field fluctuation variance.

 $\vec{a}$  = the vector of unknown interpolation coefficients,  $a_k$ , k = 1 to n.

 $\vec{s}$  = the vector of correlations between location x and location  $x_k$  (k=1 to n) with entries  $E[h h_k]$  over  $E[h^2]$ .

Equation (E9) is a system of and n equations in n unknowns. Notice that the only dependence on location x is in the right-hand side  $\vec{s}$ .

#### Kriging as a form of Optimal Interpolation

Note that (E9) is very similar to D. Morison's "Kriging\_7" equation (12) for simple Kriging:

$$0 = -\left[z\mathbf{Z}_{j}\right] + \left[\mathbf{Z}_{j}\mathbf{Z}_{i}\right]\mathbf{W}_{i}$$
(DM12)

or

$$\mathbf{R}_{\kappa}\vec{a} = \vec{s}_{\kappa} \tag{DM12b}$$

where  $\mathbf{R}_{K} = \begin{bmatrix} \mathbf{Z}_{j} \mathbf{Z}_{i} \end{bmatrix}$  is the covariance matrix of observations,  $\vec{a} = \mathbf{w}_{i}$  is the vector of weights, and  $\vec{s}_{K} = \begin{bmatrix} z\mathbf{Z}_{j} \end{bmatrix}$  is the vector of covariances between heights at location x and locations  $x_{j}$ .

The Kriging equation (DM12) is similar to (E4) and the vector of weights would be the same, but the covariances are not normalized by the variance of the heights  $E[h^2]$ , i.e.,  $\mathbf{R}_{\mathbf{K}} = \mathbf{R}E[h^2]$  and  $\vec{s}_k = \vec{s}E[h^2]$ . Perhaps more importantly for our application, Kriging makes no *a priori* distinction as to measurement noise so that in Kriging, variability due to measurement noise and the natural variability of the measured variable are mixed together at the measurement locations; essentially,  $\mathbf{R}_{\mathbf{K}} = \mathbf{R} + \mathbf{D}$  of equation (E9).

With ICESat-2 ATL12 SSH and ATL19/23 gridded DOT data we have calculated uncertainties, which are essentially the measurement errors for the mean SSH in ATL12 ocean segments and grid-cell averages of DOT in ATL19/23. Therefore, in principle, we can take advantage of Equation (E4) because we have a formalism for distinguishing between measurement noise,  $\boldsymbol{D}$ , and process variability,  $\boldsymbol{R}$ , in the analysis.

### **Elements Needed for Optimal Interpolation of ICESat-2**

To summarize, what do we need to get the coefficients to use (E1) to optimally interpolate data? We need (1) a background or prior estimate of the height,  $\mathbf{B}$ , as a function of the dimensional variable or variables, x or x, y, z, (2) a square correlation matrix of the observations,  $\mathbf{R}$ , (3) a diagonal matrix of measurement errors or uncertainties,  $\mathbf{D}$ , and (4) a nx1 vector of correlations between the interpolant points and the observation points,  $\vec{s}$ .

Background, **B** – The background field, **B**, can in principle be anything that has a mean equal to the mean of the observations. However, if the mean of the observations is used for the background, all of the variability even out to the largest scales will be included in the correlation matrix, **R**. This is unrealistic when the data domain is the global ocean, especially when we want to interpolate over a short distance, e.g., 25 km, and the physical process we want to examine has a correlation length constrained by physics. For example, the DOT measured in the Southern Ocean has nothing to do with interpolating to a 25 km grid off the coast of Greenland. In this case it makes sense to choose as a background field a climatology averaged over larger space and time scales, for which simple averaging can be

done with minimal interpolation. The pertinent example is the 9-cell, 3-month averages of ICESat-2 DOT to cell centers (e.g., Figure 8, right). These can be done monthly and for almost every grid cell. And the 91-day repeat cycle of ICESat-2 is such that the 9-cell, 3-month averages have the potential for at least one satellite pass over every grid cell, so only cells under virtually perpetual cloud cover will need to have background values interpolated to them. At least initially this can be done with simple linear interpolation, and then be iterated with near optimal interpolation coefficients from prior iterations.

<u>Correlation Matrix</u>, R - R is the covariance or correlation (the difference being the correlation matrix is covariance matrix divided by the variance) for the true data. Because we don't actually know the true data anywhere but in particular at the point to which we want to interpolate, we have to have a model of the covariance matrix based on the covariance of observations. These can be the observations that we want to interpolate or observations in the same or similar locations made in the past. In solving equation (E4) we can use the R of the actual observations to be interpolated. However, we don't have that luxury for covariances between the data points and the points with no data,  $\vec{s}$ . To make it generally applicable, the covariance matrix rests on a data-based model of the correlation of the variable as a function of separation in the relevant dimensions over which it is being interpolated, for example a Gaussian or decaying exponential with separation distance.

Following Kriging7\_JM, we can derive the covariance model using the observed covariogram  $E[h_jh_k]$  and  $E[hh_k]$  (or  $[\mathbf{Z_jZ_i}]$  and  $[z\mathbf{Z_i}]$  in the parlance of Kriging7\_JM). These are assumed to be dependent on only the separation between observation points and are therefore represented by a model of the covariogram equal to  $E[h_jh_k]$  evaluated as a function of the distance,  $d_{jk}$ , separating observation locations j and k,:

$$\mathbf{C}_{jk} \left( d_{jk} \right) = E \left[ h_j h_k \right] \tag{E10}$$

where  $C_{jk}(d_{jk})$  is the covariogram of the observations sorted by distance between observation locations.

Although  $E[h_jh_k]$  and  $E[hh_k]$  are in principle covariances of the true height values, the covariogram models are based on the observations at the observed locations. If we have a data set with the same spatial statistics as the variable we are interested in interpolating, or if there are sufficiently representative observations in the data set of interest, we can construct a sample covariogram. For every possible pair of values in the sample data, we calculate the product of the values of each sample pair as a function of the distance between each sample pair. For example, from the column vector of observation,  $\vec{h}$ , we can form the symmetric covariance matrix,  $C_H$ :

$$\boldsymbol{C}_{jk} = \vec{h}\vec{h}' = \begin{pmatrix} c_{11} & \dots & c_{1n} \\ \vdots & \ddots & \vdots \\ c_{n1} & \dots & c_{nn} \end{pmatrix}$$
(E11)

We also form the symmetric matrix of separation distances  $D_{ik}$ :

$$\mathbf{D}_{jk} = \left( \begin{array}{ccc} d_{11} & \dots & d_{1n} \\ \vdots & \ddots & \vdots \\ d_{n1} & \dots & d_{nn} \end{array} \right)$$
 (E12)

where  $d_{jk}$  equals the distance between observation points j and k. We then take all the values,  $c_{jk}$ , in the upper right half and diagonal of  $C_{jk}$  paired with the corresponding  $d_{jk}$ , and order them in ascending values of  $d_{jk}$ . The resulting array of covariance values versus separation distance can be fit with a functional model of correlation versus distance. The most common forms are decaying exponentials or Gaussians.

$$C_{V}(d) = C_{oeff} e^{\left(-d/L\right)}$$
(E13)

or

$$C_{V}(d) = C_{oeff} e^{\left(-0.5(d/L)^{2}\right)}$$
(E14)

with correlation length scale, L, and coefficient,  $C_{oeff}$ , to be adjusted to fit the covariance versus separation distance data.

Note that if we thought the correlations were different for separations in two different

directions we could fit  $\mathbf{C}_{jk}(d_{xjk},d_{yjk}) = [h_jh_k]$  as a function of  $d_x$  and  $d_y$  to get a model  $s_x$  and  $s_y$  and covariogram  $V(d_x$  and  $d_y$ ), exponential:

$$C_{V}\left(d_{x},d_{y}\right) = C_{oeff} e^{-k_{x}d_{x}} e^{-k_{y}d_{y}}$$
(E15)

or Gaussian:

$$C_{V}\left(d_{x},d_{y}\right) = C_{oeff} e^{\left(-0.5\left(d_{x}/s_{x}\right)^{2}\right)} e^{\left(-0.5\left(d_{y}/s_{y}\right)^{2}\right)}$$
(E15)

<u>Interpolant Correlation Vector</u>,  $\vec{S}$  - The vector  $\vec{S}$  is the vector of correlations between location x and location  $x_k$  (k=1 to n) with entries  $E[h h_k]$  over  $E[h^2]$ . In this case we

absolutely have to have the model of covariance, because by definition there are no data for h at the interpolant point. For example, using an exponential model of the covariogram for  $\vec{S}$  we set

$$\mathbf{C}_{j}(d_{j}) = E[hh_{j}] = C_{oeff} e^{(-d_{j}/L)}$$
(E16)

where  $C_j(d_j)$  is the model covariogram as a function of the distance,  $d_j$ , between the observation locations and the location of the point to be interpolated. Note that if the constellation of measurement points was changed, for example made smaller to interpolate closer to a coastline, the same modeled correlation function from the original covariogram could be used with a smaller subset of the original observation points to form R.

Measurement Error Matrix D – The matrix D is the diagonal matrix with entries  $\sigma_k^2/E[h^2]$ . Because the correlation of the true h(x) with itself is 1, the diagonal elements of  $R_K = R + D$  are going to be equal to the natural variance of h as a function of location plus the measurement variance. When we use the covariogram of observations to model  $R_K$ , the diagonal elements will devolve into a constant that includes natural variability and the variance due to measurement noise. Our known uncertainties from ATL12 will not enter into determining the optimal interpolation coefficients for the surface height anomalies about the background. However, we can examine the fit of the covariogram for small separation distances and extrapolate to zero separation. This will give an estimate of the average of the natural or true variance at zero separation, i.e., the diagonal elements of R. The difference between the covariance extrapolation to zero separation and the observed covariance at zero separation should be similar to the uncertainties from ATL12. If it is not, we may choose to adjust the fit to the covariogram data by subtracting the average measurement noise from the covariogram data at zero separation. The resulting model R can be compared with the covariances estimated from ocean models and other observations.